Quaternary Research

doi:10.1017/qua.2019.68

Tectonism and volcanism enhanced by deglaciation events in southern Iceland

Brigitte Van Vliet-Lanoë[a]*, Françoise Bergerat[b], Pascal Allemand[c], Christophe Innocentd[d], Hervé Guillou[e], Thibault Cavailhes[f], Águst Guðmundsson[g], Gilles Chazot[a], Jean-Luc Schneider[f], Philippe Grandjean[d], Celine Liorzou[a], Sophie Passot[d]

[a]IUEM-Université de Bretagne Occidentale, CNRS UMR 6538 Géosciences Océan, 29280 Plouzané, France
[b]Institut des Sciences de la Terre de Paris, Sorbonne Université, CNRS, UMR 7193, Paris, 75005, France
[c]Laboratoire de Géologie de Lyon LGLTPE, Université Lyon 1 and ENS-Lyon, 2, CNRS, UMR 5276, Villeurbanne, 69622 Cedex, France
[d]Bureau des Recherches Géologiques et Minières (BRGM)–LAB/ISO, Orléans; 45060 Cedex 2, France
[e]LSCE UMR 8212, CNRS-CEA, Bât. 12, Domaines CNRS, Gif/Yvette, 91198, France
[f]EPOC, UMR 5805 CNRS and Université de Bordeaux, 33615 Pessac Cedex, France
[g]Jarðfræðistofan ehf, Hafnarfjorður, 221, Iceland
*Corresponding author e-mail address: brigitte.vanvlietlanoe@univ-brest.fr (B. Van Vliet-Lanoë).

(Received January 1, 2019; Accepted September 30, 2019)

Abstract

Southern Iceland is one of the main outlets of the Icelandic ice sheet and is subject to seismicity of both tectonic and volcanic origins along the South Iceland Seismic Zone (SISZ). A sedimentary complex spanning Marine Isotopic Stage 6 (MIS 6) to the present includes evidence of both activities. It includes a continuous sedimentary record since the Eemian interglacial period, controlled by a rapid deglaciation, followed by two marine glacioisostasy-forced transgressions, separated by a regression phase connected to an intra-MIS 5e glacial advance. This record has been constrained by tephrostratigraphy and dating. Analysis of this record has provided better insights into the interconnectedness of hydrology and volcanic and tectonic activity during deglaciations and glaciations. Low-intensity earthquakes recurrently affected the water-laid sedimentation during the early stages of unloading, accompanying rifting events, dyke injection, and fault reactivations. During full interglacial periods, earthquakes were significantly less frequent but of higher magnitude along the SISZ, due to stress accumulation, favored by low groundwater levels and more limited magma production. Occurrence of volcanism and seismicity in Iceland is commonly related to rifting events. Subglacial volcanic events seem moreover to have been related to stress unlocking related to limited or full unloading/deglaciation events. Major eruptions were mostly located at the melting margin of the ice sheet.

Keywords: Glacio-isostatic rebound; Tectonism; Seismicity; Volcanic activity; South Iceland Seismic Zone

INTRODUCTION

Iceland is an emerged, slow-spreading part of the Atlantic oceanic ridge–rift system, under the control of a hot spot underlying two different plates that host overlapping volcanic zones, both subject to plate tension. Iceland has also been covered, completely or partially, by ice since the Pliocene (3 Ma), having had a large ice cap since 2.2 Ma (Geirsdottir and Eiriksson, 1994).

Most of the tectonic and seismic activity in Iceland is connected via fissure systems and is generated by hot-spot volcanism with correlation between volcanic activity in the East Volcanic Zone (EVZ) and Holocene seismic activity in the western South Iceland Seismic Zone (SISZ; Larsen et al., 1998). More specifically, during the Holocene, the SISZ (Fig. 1C) accommodated left-lateral transform movement between the West Volcanic Zone (WVZ) and the more active EVZ (Fig. 1). This transform zone included N–S right-lateral strike-slip faults that largely controlled seismicity during the Holocene (Einarsson and Eiríksson, 1982; Stefánsson et al., 1993).

Global volcanism seems to be influenced by Milankovitch cycles (Kutteroff et al., 2013). The 1.8 and 5 ka tidal cyclicities of the solar system that induce some deformations in the lithosphere also modulate the climate in synchronicity with the warming leading to Dansgaard-Oeschger (DO) ice-rafted

Cite this article: Van Vliet-Lanoë, B. *et al* 2020. Tectonism and volcanism enhanced by deglaciation events in southern Iceland. *Quaternary Research* 94, 94–120. https://doi.org/10.1017/qua.2019.68

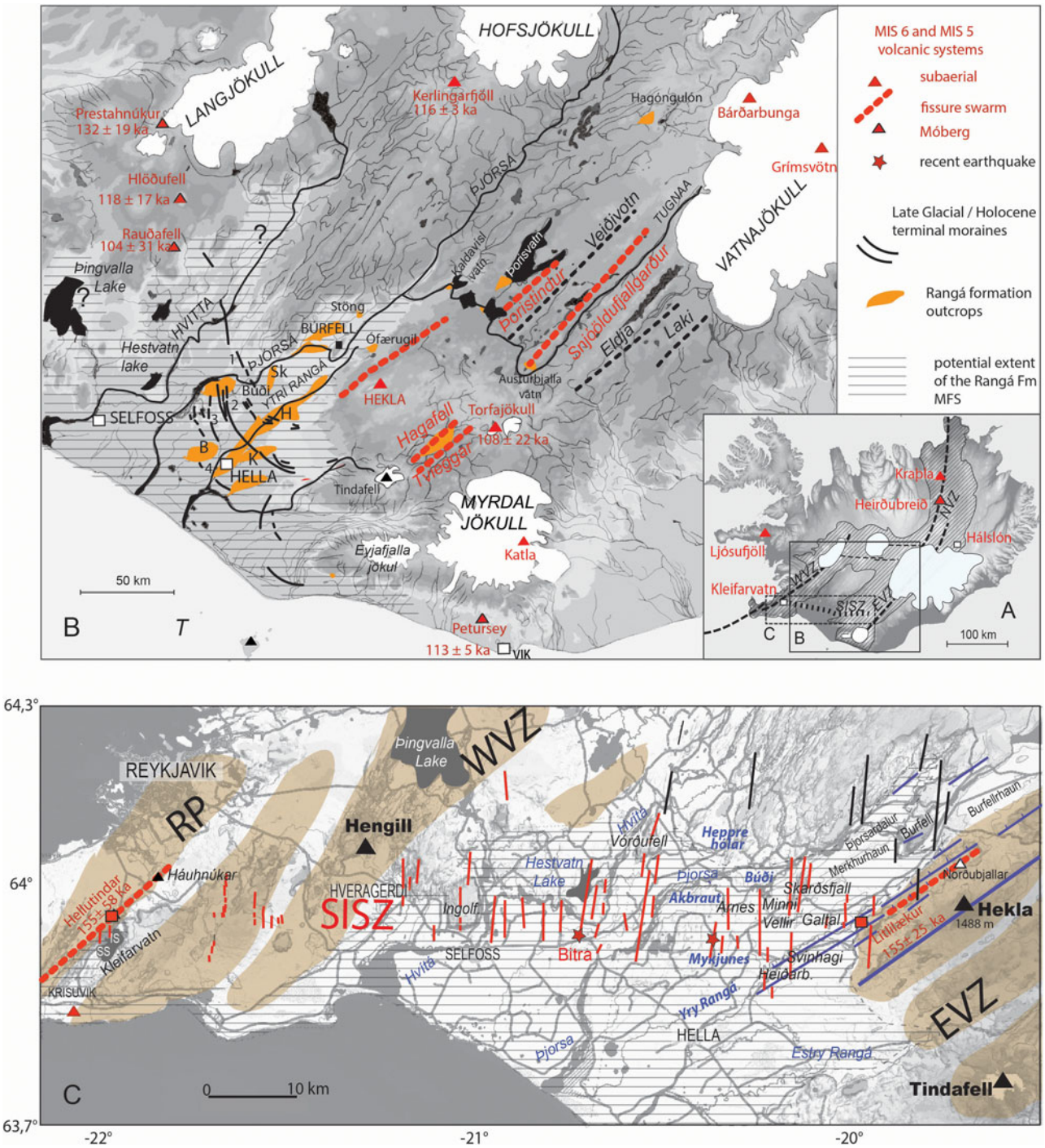

Figure 1. Location of the investigated sites: (A) general view and (B) extent of the interglacial formation. Morainic arc complexes: 1, Finse-Búði; 2, Mykjunes; 3, Litlatunga; 4, Sólvellir. Investigated sites: B, Bolstaður; K, Kirkjubær; H, Heiðarbrekka; Sk, Skarðsfjall; Stöng, archaeological site; O, Ofærugill. WVZ, West Volcanic Zone; EVZ, East Volcanic Zone; NVZ, North Volcanic Zone; SISZ, South Iceland Seismic Zone. (C) SISZ in relation to the interglacial formation estuaries and volcanic systems (in khaki). Names of late-glacial morainic arcs given in blue. IS, Innristapi; SS, Syðristapi; RP, Reykjanes Peninsula. White triangles, tuyas; Red stars, AD 2000 twinned earthquakes (modified and completed from http://www.norvol.hi.is/~thora/olfus.html). Note the Hekla flexural zone in violet. SISZ: historical and present-day active faults in red, inactive in black. For the ages (in red) see Table 3, Supplementary material (For interpretation of the references to color in this figure legend, the reader is referred to the web version of this article.)

debris (IRD) cycles (Keeling and Whorf, 2000). It is therefore not surprising to find a reasonable correlation in Iceland between the warmings and tectonic events that control the volcanic activity. Little is known concerning the timing of volcanic activity during ice-sheet building. Most subglacial activity is commonly attributed to the last glacial maximum

https://doi.org/10.1017/qua.2019.68 Published online by Cambridge University Press

(LGM) or its deglaciation (Walker, 1965; Licciardi et al., 2007; Eason et al., 2015), which conflicts with the Plio-Pleistocene glacial history of the island (Geirsdottir and Eiriksson, 1994).

Based on the Reykjanes Peninsula postglacial volcanism study, Guðmundsson (1986) suggested that the rapid uplift and bending of the crust above the magma reservoirs, during the glacial unloading, favor the formation of ridges and shield volcanoes. Since that time, the mechanical effects of deglaciation on volcanism and the connection between glacial loading/unloading and volcanic activity have been discussed, analyzed, or modeled by many (Jull and McKenzie, 1996; Slater et al., 1998; Zielinksi, 2000; Maclennan et al., 2002, Sinton et al., 2005; Andrew and Guðmundsson, 2007; Huybers and Langmuir, 2009; Sturkell et al., 2003; Praetorius et al., 2016). Glacial unloading is thought to have been responsible for an increase in magma melting rates below the base of the crust, due to enhanced mantle decompression (Maclennan et al., 2002; Sinton et al., 2005), in combination with unloading by subglacial erosion (Sternai et al., 2016). This resulted in a significant percentage of global volcanic eruptions during the early stages of deglaciation (Watt et al., 2013; Rawson et al., 2016), between ~13 ka and 11 ka, followed by an intensification at 10.3 ka, expressed by the Saksunarvatn eruption (Grímsvötn; Zielinksi, 2000; Eason et al., 2015). The return to normal occurred progressively after 10.3 ka (Sinton et al., 2005; Eason et al., 2015).

Unconsolidated deposits from the last deglaciation in southern Iceland (Fig. 1B) have been well studied (Van Vliet-Lanoë et al., 2018), and the sedimentary deposits, with evidence of volcanic activities, are commonly faulted and have convoluted bedding of possible co-seismic origin,. Very few sequences recorded the last interglacial near 60°N latitude. The Rangá Formation, in southern Iceland (63°–64°N; Van Vliet-Lanoë et al., 2018), is an extended sequence, including an estuarine Marine Isotopic Stage 5e (MIS 5e) complex preserved below the well-studied deposits of the last deglaciation. This long record crosses the SISZ and thus could provide information to link the ice-sheet dynamics, the underlying geodynamics, and the volcanic activity. In particular, it includes potentially datable lava and tephra. The complete sedimentary sequence has been fully described, and its significance, in terms of paleoclimate, has been discussed (Van Vliet-Lanoë et al., 2018). As the SISZ is the most active onshore seismic zone in Iceland, it is the best place to determine any changes in seismicity or tectonic style following the strain imposed by glacial loading/unloading and any associated hydrological changes.

We consider, in this paper, the lastest and prior deglaciations as having temporarily enhanced volcanism. The aim of this work was, first, to attempt to understand from this extended sedimentary record the relationship between glaciations and volcano-seismo-tectonic activity along the SISZ (Fig. 1C). In this study, we focused on the 160–155 ka (MIS 6b) deglaciation, the Termination IIb (132 ka), the deglacial event (116 ka), the GI 25 of the Greenland ice cores, and Terminations Ia and Ib (14.5 and 12 ka, respectively). To understand the specific impacts of glacial loading, we examined the connection between the characteristics and the ages of the subglacial volcanoes (tuyas, or hyaloclastite ridges), from volcanic zones, using radiometric dating, facies, and the tephrochronological record from marine and glacial cores.

METHODS

Sedimentological studies in the Ytrí Rangá valley, and on surrounding volcanoes, were conducted from 2004 to 2018; the Lake Kleifarvatn system was analyzed in 2009 through 2017. Our observations are based on detailed mapping and section descriptions (see Van Vliet-Lanoë et al., 2018, Supplement 1, and site locations in Table 1 of the Supplementary material). The station locations were obtained by Global Positioning System measurements, which were compared with the revised topographical map of Iceland (http://kortasja.lmi.is, 2014 and 2018), giving an average vertical error of ± 5 m. Tectonic studies of Quaternary to present-day faulting, based on both field studies and the focal mechanisms of earthquake analysis, were conducted in the EVZ and SISZ from 1995 to 2016. High-resolution aerial views and digital elevation models (DEMs) were produced using a drone (a Naza hexacopter). This allowed stereoscopic overlapping to construct a high-resolution and interactive DEM using the MicMac computer program specifically developed at Lyon I University (Pierrot-Deseilligny and Paparoditis, 2006, see Supplementary Material). As a result, we expected to obtain DEMs and Orho-images at a resolution of better than 3 cm.

Petrographic analyses (thin sections, X-rays, scanning electron microscopy, geochemistry, inductively coupled plasma mass spectrometry (ICPMS AEL) were performed using the procedure outlined by Cotten et al. 1995). Trace element concentrations on tephra and lava were also measured with a Thermo Element2 HR-ICP-MS in Brest (France), after repeated HF-$HClO_4$ digestion and HNO_3 dilutions (for details, see Li and Lee, 2006). Major elements were analyzed using the Brest CAMECA CAMEBAX SX100 electron microprobe with a specific protocol (see Supplementary Material, p. 11).

All the used K-Ar and $^{40}Ar/^{39}Ar$ dating are taken from previously published data (see Supplementary material, Table 3) produced using the methodology established by Guillou et al. (2010, 2019). Reliable data for the Galalaekur lava were not available, so U-Th dating was performed on lavas from the Rangá valley at BRGM Orléans on a Neptune MC-ICPMS. Details on chemical separation and mass spectrometry can be found elsewhere (Innocent et al., 2005; Millot et al., 2011). A reference age of 116 ka was derived, although no well-defined isochron could be obtained. Calculations were done using the method of Minster et al. (1979; see Supplementary Material, p. 8).

An attribution of the Rangá Formation to the MIS 5 sensu lato (MIS 5e and 5c, Member C) was measured using a uranium isotope desiquilibrium methodology (see Supplementary Material, p. 7), yielding an age of 116 ka on lava interstratified in the C3 unit. The radiometric ages (K–Ar ages) of the same units in Snafelness (132 and 129 ka) and

https://doi.org/10.1017/qua.2019.68 Published online by Cambridge University Press

in the Southwestern Volcanic Zone confirm this attribution (see Van Vliet-Lanoë et al., 2018). It has also been confirmed by the tephrostratigraphic signature of the outcrops, which is consistent with the available regional data from marine and ice records (Davies et al., 2014). The timing of the Grímsvötn, Bárðarbunga, and Hekla volcanic eruptions from MIS 5e to the present was compiled from a published, synthesized tephrostratigraphic series (Óladóttir et al., 2011; Davies et al., 2014; Voelker and Haflidason, 2015). As a complement, we report in the Table 3 of the Supplementary Material the available K–Ar and $^{40}Ar/^{39}Ar$ ages spanning the same interval and performed on subglacial (tuyas) and subaerial lavas. These ages are crucial for constraining the dynamics of the last large Icelandic ice sheet interacting with volcanic activity.

Regional geological setting of the extended sedimentary record

South-central Iceland is a wide depression, delimited by two volcano-tectonic zones—the WVZ to the west and the more active EVZ to the east (Fig. 1A). The EVZ is the youngest part of the Icelandic rift, and has been active since 2–3 Ma (Johannesson et al., 1990). It includes, among others, the Katla, Torfajökull, Hekla, and Tindafell Volcanoes. This depression is one of the main outlets for the Icelandic glaciers. The central plain is formed by a complex sandur, related to the Ytrí Rangá, Þjórsá, and Hvítá Rivers (Fig. 1B). It was regularly scoured by late-glacial/Holocene jökluhlaups—or flash floods—that were often triggered by the subglacial volcanic activity (Björnsson, 2002). Late-glacial and Holocene lava flows also partly protected the old sediments, allowing for good outcrop exposures.

Overview

The south-central Icelandic depression is characterized by the presence of interstratified basalts and glacial and hyaloclastite deposits, ranging in age from early Quaternary to Holocene (Johanesson and Sædmundsson 1998; Kristjánsson et al., 1998; Fig. 1B). Regional volcanic activity increased during the last deglaciation, especially for the Grímsvötn, Bárdarbunga, and Katla Volcanoes, with Hekla apparently showing activity later, close to 6060 cal yr BP (Larsen et al., 2002; Guðmundsdottir et al., 2016). The most widespread early Holocene lava inside the central zone is the Þjórsá Lava flow field (Fig. 1C), dated ca. 8.6 ka (Hjartarson and Ingólfsson, 1988; Halldorsson et al., 2008), which issued from the Veiðivötn fault system (Bárðarbunga volcanic system; Fig. 1B). These lava flows capped most of the older sediments, previously considered to be Holocene in age (Einarsson, 1994) and also postdate the Búði Preboreal moraine system (11.2 ka: Geirsdóttir et al., 2000; Fig. 1B).

South Iceland Seismic Zone

Southern Iceland is crossed from west to east by the SISZ (Fig. 1C), a transform zone that extends inland from the Reykjanes Peninsula (Fig. 1C), which represents the extension of the present-day Reykjanes Ridge (analyzed at Kleifarvatn; Clifton et al., 2003), and ends to the east with the Torfajökull volcanic system and probably the Laki fissure eruption (Jakobsdóttir, 2008). The largest present-day earthquakes in Iceland occur within the SISZ (e.g., magnitude 6.6 in June 2000), which comprises a Riedel shear zone, where several sets of shear fractures rupture during earthquakes. Most present-day major seismic events (moment magnitude [Mw] > 5) are located in the western part of the SISZ (Jakobsdóttir, 2008), from the Hengill Volcano to Lake Kleifarvatn (Hjaltadóttir, 2009), where volcanic activity is low today, as well as in the Reykjanes Peninsula.

Despite the general E–W trend of the SISZ, the majority of present-day earthquakes occur along N–S-trending faults (e.g., Rögnvaldsson and Slunga, 1994; Slunga et al., 1995; Decriem et al., 2010), suggesting that the left-lateral transform movement is, to a great extent, accommodated by right-lateral displacement along these N–S strike–slip faults, achieved by relatively shallow earthquakes (2–6 km on average with a maximum 10 km depth). The shallowness of this earthquake activity increases its sensitivity to the presence of the water table. Trigger earthquakes, which are the largest-magnitude earthquakes to occur in Iceland (Mw > 5), are commonly followed by a cluster of lower-magnitude events in the following days or months (Decriem et al., 2010), usually in connection with a temporarily raised water table (Jónsson et al., 2003).

Historic earthquakes are mainly expressed in the field as large N–S-trending faults arranged side by side (e.g., Einarsson and Eiriksson, 1982; Einarsson, 1991; Bergerat and Angelier, 2003; Einarsson et al., 2005; Bergerat et al., 2011; Fig. 1C), but left-lateral seismic faults also exist in the present day (e.g., Angelier and Bergerat, 2002) and occurred during historical periods and earlier (e.g., Bergerat et al., 2003, 2011; Guðmundsson, 2017). Measurements on basaltic rocks (dated at 0.8–3.3 Ma) cropping out along the Þjórsá River (Bergerat and Plateaux, 2012) exhibited N45°–N65° (left-lateral) and N10°–E35° (right-lateral) strike–slip faults and N40°–N55° normal faults and veins. Broadly speaking the NE–SW trends correspond to the normal faults and dykes of the volcano-tectonic systems. The expanded sedimentary sequence in the Ytrí Rangá valley corresponds to the crossing zone between the SISZ known seismic faults (Skarðsfjall and Minnivellir; Fig. 1) and the Hekla fault system.

Main volcanic systems

Until now, only three main volcanic sources have been identified through geochemical analysis of tephra and lava from the MIS 5e sedimentary Member C (units C1 to C6) in the Rangá Formation—the Grimsvötn, Bárðarbungá, and Hekla Volcanoes.

The Grímsvötn volcanic system consists of six en échelon fault systems which are between 150 and 190 km in length and central volcanoes. The Grímsvötn Volcano itself is

https://doi.org/10.1017/qua.2019.68 Published online by Cambridge University Press

located at the apex of the Icelandic hot spot, some 150 km NE of the Hekla Volcano (Fig. 1). This seems to have been the most active volcano during the Holocene (Larsen et al.,1998; Óladóttir et al., 2011). Its eruption frequency is mostly ca. 10 yr, with an intensity ruled by a 60 to 80 yr cyclicity (Óladóttir et al., 2011). Weichselian activity has been recognized in marine and ice cores down to 127 ka (Davies et al., 2014; Voelker and Haflidason, 2015). The volcano appears to have two reservoirs—a shallow one at ca. 3 km depth and a deeper one at 15 km (Reverso et al., 2014). The shallow depth of the upper reservoir makes it potentially highly sensitive to rapid unloading resulting from deglaciation events (Höskuldsson et al., 2006). For example, the complex Saksunarvatn tephra (10.4 to 9.9 cal ka BP; Johannsdottir, 2007) is related to the drainage of the Vatnajökull subglacial lakes or aquifers and the following incomplete deglaciation and rebound of the Erdalen cold events (Van Vliet-Lanoe et al.unpublished). It is connected to a fault system that was responsible for the Laki and older eruptions. This caldera is covered by about 400 m of ice (Bjornsson, 2009). The subglacial topography of Vatnajökull shows a large triple caldera—a major source of jökluhlaups (Björnsson, 2002).

The Bárðarbunga Volcano forms a wide caldera, located at the northwestern edge of the Vatnajökull ice cap, that is filled by about 400-m-thick ice (Bjornsson, 2009). This volcano is located along a large fault system—the Veiðivötn—that parallels the Grimsvötn system but also continues to the northern coast of the island (North Volcanic Zone). Its lavas are tholeiitic in composition. The reservoir is located at about 12 km depth (Guðmundsson et al., 2016). During the Holocene, the eruption frequency was 5 eruptions/100 yr (Óladóttir et al., 2011), also recognized in marine tephra down to 110 ka (Davies et al., 2014; Voelker and Haflidason, 2015). This volcano is now emerging from the ice sheet. Due to its wide caldera, it is a major source of jökluhlaups, especially in the southern embayment (Björnsson, 2002).

The Hekla Volcano is an andesitic stratovolcano (Sigmundsson et al., 1995). Its summit reaches 1488 m above sea level (m asl), and it is located on an independent fault system. It is presently sparsely covered by glaciers. The positioning of Hekla corresponds, more or less, to the crossing of this fault system with the SISZ. It has only one deep reservoir, from 14 km to 20 km in depth (see synthesis in Reverso et al., 2014). Holocene activity was very frequent (Oladottir et al., 2011), recognized in marine tephra down to 80 ka (Davies et al., 2014; Voelker and Haflidason, 2015). The onset of the Hekla Volcano is much older, dating at least back to ca. 417 ka ($^{40}Ar/^{39}Ar$ age of feldspar; Van Vliet-Lanoë et al., 2018) and lava and pumices are recorded within the MIS 5e record.

Glaciers

The larger Icelandic glaciers today are mostly polythermal and are frequently (66%) subject to surge dynamics (Björnsson et al., 2003; Björnsson, 2009). Their motion is somewhat helped by the presence of subglacial lakes (Björnsson, 1998; Auriac et al., 2014). Glaciers are supposed to have completely disappeared during the Holocene thermal optimum (ca. 8 ka; Ingólfsson, 1991; Striberger et al., 2012), but were restored from 4.5 ka. Nevertheless, while this disappearance may have been the case for small glaciers, such as Eyafjallajökull, it is likely that certain glaciers subsisted on western Vatnajökull, and probably on Langjökull and Hofsjökull, during the optimum (Flowers et al., 2007, 2008; Björnsson, 2009). The phreatomagmatic character of the MIS 5e 5e-low/BAS tephra in the Rangá Formation (Van Vliet-Lanoë et al., 2018) suggests the persistence of some ice during the thermal optimum of the last interglaciation. The age of the tuyas south of the Langjökull ice cap (Van Vliet-Lanoë et al., 2018: Table 1) also suggests an early re-extension of this ice cap (MIS 5d). The last deglaciation proceeded from the Bölling interstade (14.5 cal ka BP), with pulsed readvances (Geirsdóttir et al., 2009) and the development of ice streams (Principato et al., 2016). The final full deglaciation (beyond the present ice extent) occurred just after 10.3 cal ka BP (Geirsdóttir et al., 2009).

Permafrost today extends mostly from elevations above 800 m asl in northern Iceland (Etzelmüller et al., 2007) and ca. 1000 m asl to the south. Sporadic permafrost is more widespread down to 600 m asl in southern Iceland. During the MIS 5e cold event (Greenland glacial stadial GS26) at Halslón, permafrost developed from ca. 600 m asl in freshly deposited tills (Van Vliet-Lanoë et al., 2010). This means that early glacier development during MIS 5e and MIS 5d was probably initially polythermal.

Sedimentary record east of the SISZ—the Ytrí Rangá valley

The sedimentary record in this region has been subdivided into several members, with Member A representing the oldest features, and Member B being a glaciovolcanic complex with a K–Ar age close to ca. 155 ka (Van Vliet-Lanoë et al., 2018; Table 3)

Member C sensu stricto (Rangá Formation) has an MIS 5 age (Van Vliet-Lanoë et al., 2018) and crops out in the Rangá and Þjórsá valleys. It is the main, and most complex, deposit of the Rangá Formation, with an average thickness of 30 m. Most of the material that comprises Member C was inherited from the subglacial eruption(s) of the Hekla Volcano and the old hyaloclastite ridges of the Veiðivötn system (Fig. 1B). The spectacular preservation of this interglacial prism is partly related to major topographical shaping by the MIS 6 ice sheet, the rapid deglaciation of Termination IIb, and the cold-based and low-erosive characters of the Weichselian glaciation (Van Vliet-Lanoë et al., 2001; Geirsdóttir et al., 2007). Members D, E, and F encompass the last glacial period, the late-glacial transition, and the Holocene period, respectively. Members E and F are much less interconnected spatially and are much thinner. With the record of a first deglaciation close to 155–150 ka at Ófærugill and Kleifarvatn, Member C in the Ytrí Rangá valley, and the late-

https://doi.org/10.1017/qua.2019.68 Published online by Cambridge University Press

glacial–early Holocene record in the south embayment, we have a long sedimentary sequence that covers at least four main deglaciation events. Detailed descriptions and interpretations of the members of this record have been reported in Van Vliet-Lanoë et al. (2018; Table 1 in Supplementary material, p. 9); a composite stratigraphic column is shown in Figure 2.

Timing

The Ofærugill Member B records a long interstadial, lasting ca. 10 ka under cool conditions, MIS 6b (162–150 ka, Zeiffen interstadial; Seidenkrantz et al., 1996), followed by the very cold MIS 6a (Kattegat stadial). MIS 6b is associated with the major retreat of all European ice sheets (Toucanne et al., 2009). The deglaciation was partial, but extensive, occurring here at least south of the Búrfell (Fig. 1B), but also in northern and northeastern Iceland based on K-Ar dates from subaerial lavas (Guillou et al., 2010). To the west, hyaloclastite ridges developed as at Kleifarvatn (dated 155 ± 58 ka).

Member C represents an interglacial period, MIS 5e–5d in age, recording a time span of ca. 129–110 ka (Van Vliet-Lanoë et al., 2018). Analysis of the uranium isotope disequilibrium yielded a date of 116 ka for the Galtalækur lava (Unit C3), with field evidence suggesting an age of 125 ka (see Fig. 2). The age of this member is confirmed on the basis of paleoclimatic correlations, the occurrence of the 127 ka Grimvötn 1/5e-low/BAS tephra (confirmed by single-grain laser ICPMS analysis; Van Vliet-Lanoë et al., 2018, Supplement 3) in Unit C3a, and the presence at Hellar Cave in upper Unit C6, of the "110 ka NGRIP 2745.6 m" tephra (Davies et al., 2014 : Grimsvötn volcanic source with a limited Katla Volcano input extracted from microprobe analysis). From the ice-core record of the North Greenland Eemian Ice Drilling project (Dahl-Jensen et al., 2013) and the Red Sea coral record (Siddal et al., 2006), the penultimate deglaciation (Termination IIb, 132–130 ka) is known to have been extremely rapid, much more so than the late-glacial deglaciation (Termination Ib). In Iceland, once initiated, this rapid deglaciation proceeded under the direct influence of the mild Irminger Marine Current. Member C is a record of Termination IIb (ca. 130–129 ka), the Eemian optimum (127 ka), the intra-Eemian cooling (GS26 of Greenland stadials, ca. 120–116 ka), and the late warming of glacial interstadial GI25 (116–113 ka; North Greenland Ice-core Project [NGRIP]; McManus et al., 2002; Andersen et al., 2004; Rasmussen et al., 2003). It preserves two successive and distinct transgressive system tracts, separated by ca. 9 ka—Estuary 1 and Estuary 2—which were forced by two successive glacioisostatic rebounds (Fig. 2) controlled by the vicinity of the main ice sheets. This internal marine regression records the distal signature of a complex glacial advance—GS26—as observed in central Iceland (Van Vliet-Lanoë et al., 2010). The Grímsvötn and Hekla Volcanoes were highly active (tephra, lapilli, and lava flows) during all the deglaciation events, confirming previous observations of Termination Ib (11 ka; Óladóttir et al., 2011). This was also true during the emplacement of Unit C6, during a brief deglaciation—Termination IIc (116–113 ka; Van Vliet-Lanoë et al., 2018).

A record of the early Weichselian ice sheet is absent from the sedimentary record in the central embayment, up to at least 110 ka (based on the Hellar Cave tephra), but one is present south of the Langjökull and Vatnajökull Ice Sheets, based on dated tuyas.

Deglaciation was important inland from 14.5 ka cal BP, with a lacustrine facies being deposited close to Hepprehólar (Geirsdottir et al., 2009), which was deformed by the Younger Dryas and Pula–Mykjunes advances, capped by the Vedde Ash (11.8 ka cal BP; Van Vliet-Lanoë et al., 2018), and finally by the Preboreal Búði moraine system (11.2 ka cal BP; Geirsdóttir et al., 2000; Fig. 1B). The sediments associated with the late-glacial and Preboreal advances are interstratified with jökulhlaup deposits, basaltic tephra, and marine deposits. The highest marine transgression during the Preboreal (Termination Ib) reached a regional elevation of 110 m asl inland in the southern Icelandic embayment, dated as ca. 11.2 ka cal BP, resuming at around 9 ka (as synthesized in Geirsdóttir et al. [2000] and Biessy et al. [2008]). The Holocene record continued with the Þjórsá Lava and sandur deposits that were covered by loess from ca. 8.5 ka cal BP and mainly sand dunes during the Little Ice Age (Jackson et al., 2005).

DATA

Paleoseismicity and fault activity along the SISZ

Paleoseismicity (Rangá Formation)

Deformed sedimentary deposits with co-seismic origins have been clearly differentiated from deformations in periglacial, glacial, and storm-wave breaking conditions on the basis of their topographic locations in basinal or more proximal settings, their drainage capability and grain size, and also their internal organization and fabric (oriented patterns, clustering in nodal positions, shortening fabrics, nontidal layer fragmentation; Van Vliet-Lanoë et al., 2004, 2005). Evidence includes the occurrence of several clustered co-seismic patterns (e.g., Fig. 3) or/and faulting affecting the same sedimentary unit(s) (e.g., Fig. 4). Their stratigraphic attributions are commonly given by the age of the affected upper boundary of the unit, except for small-sized synsedimentary patterns. This approach has not been applied to volcanogenic sedimentary sections in connection with existing fault zone (Fig.5).

Two types of paleoseismic records have been observed.

Type 1. Low surface-magnitude earthquakes: Evidence of recurrent low surface–magnitude (Ms) seismicity includes small (<25 cm) water-escape structures (Obermeier, 1996; Fig. 3A), small loadcasts (Sims, 1975; Van Loon, 2009; Fig. 3F), oriented loadcasts in nodal position (Van Vliet-Lanoë et al., 2004; Fig. 3E), Kelvin–Helmholtz subaqueous instabilities (Heifetz et al., 2005), and dish-and-plate

https://doi.org/10.1017/qua.2019.68 Published online by Cambridge University Press

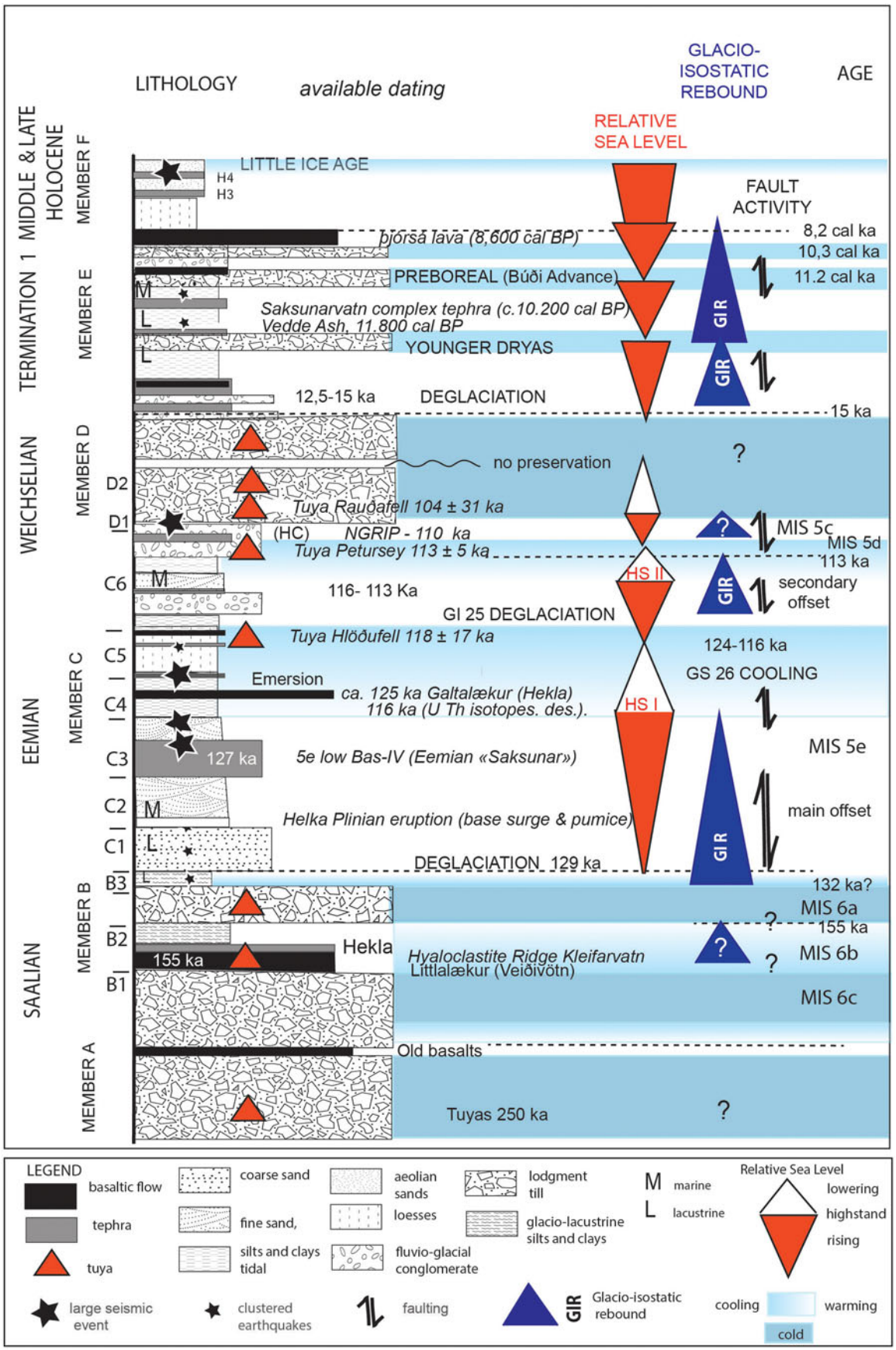

Figure 2. (color online) Composite log of the Rangá Formation. Large seismic events correspond to ruptures in the field. Clustered earthquakes correspond to low-magnitude events (Ms < 5).

https://doi.org/10.1017/qua.2019.68 Published online by Cambridge University Press

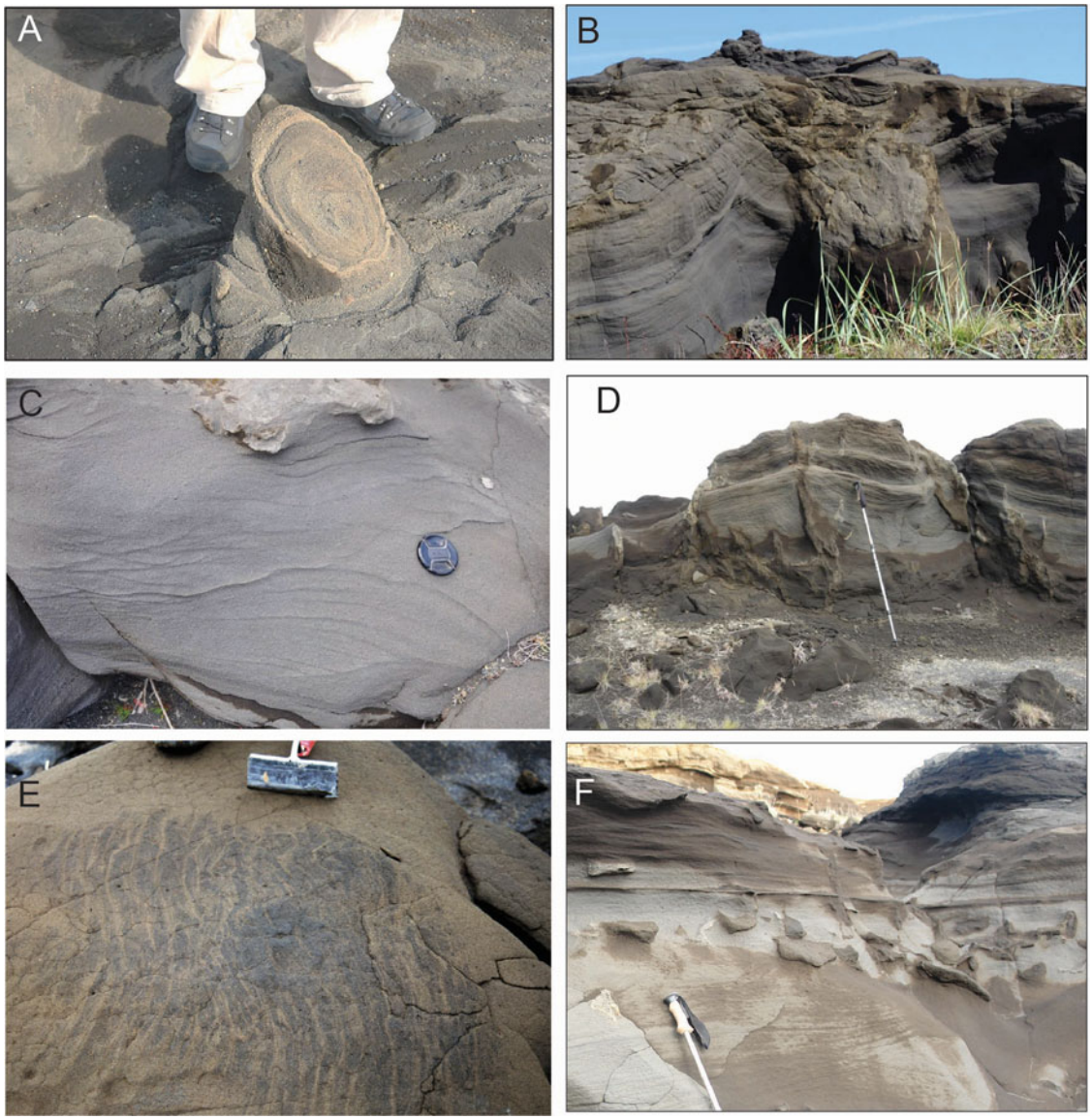

Figure 3. (color online) Low-intensity co-seismic sedimentary deformations at Heidarbrekka West: (A) Unit C2; (B) Unit C3a, synsedimentary water escape that reworked C2 material and was emitted from the top of Unit C3a; (C) dish structures disturbing the stratification (Unit C3a); (D) flame structures or injections of Unit C2 material along fractures (SISZ) in Unit C3a; (E) oriented and clustered microloads in early Unit C4; (F) Synsedimentary and clustered loadcasts of the Grim 1 redeposited tephra in Unit C3a.

structures (Lowe and LoPiccolo, 1974; Fig. 3C) during the deposition of Units B2 and B3 (ca. 155–150 ka, deglaciation event) and C1 and C2 (ca. 129–127 ka; Fig. 2) of the Ytrí Rangá long sequence (Van Vliet-Lanoë et al., 2018). Co-seismic synsedimentary layer fragmentation (Owen et al., 2011) is uncommon in the Rangá sediments, as are layer stretching and disruption. This is related to the low-angled slopes in the paleo-estuary compared with their frequency in the incised valleys of northern Iceland (Van Vliet-Lanoë et al., 2005).

These events are synchronous with the first transgressive event within MIS 5e (Termination IIb). A similar situation also prevailed during the inundation of Termination Ib at Akbraut, between ca. 11.2 (from ^{14}C) and 11.4 cal ka BP (Figs. 1C, 4C), with synsedimentary fragmented layers and small loadcasts in association with some limited activity in the SISZ fault system (see Supplementary Material).

Type 2. High surface–magnitude earthquakes: Large MIS 5e earthquakes have mostly been recorded in the Ytri Rangá valley. At least two successive seismic crises were recorded during emplacement of Units C3–C4 (Figs. 3, 6D, and 7B) at Heiðarbrekka. Plurimetric convolutions were observed at Kirkjubær (Fig. 1), with shortening figures (Fig. 7B), just below the second transgression surface (base of Unit C6).

The earthquake evidence at the top of Unit C4 (ca. 126–125 ka; Fig. 6D) was associated with evident ruptures in the SISZ (Fig. 1C) and superficial folding (Fig. 7A, basaltic tephra He 2 in C4), synchronous with the hydrostatic unloading resulting from the first regression. It should be

https://doi.org/10.1017/qua.2019.68 Published online by Cambridge University Press

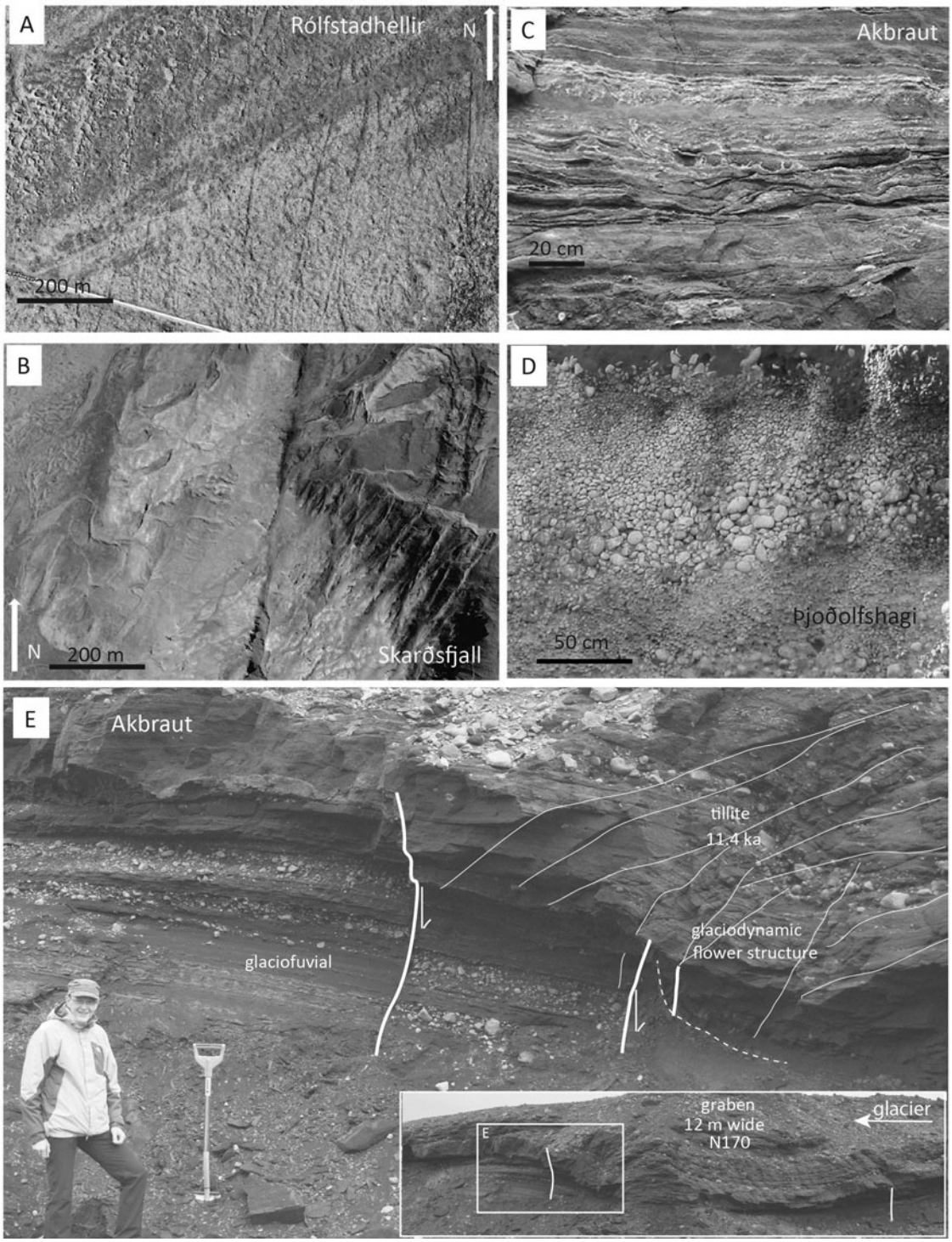

Figure 4. Faulting and co-seismic activity during the late-glacial period and early Holocene (Member F). (A, B) SISZ faults from aerial views (N10°E in lavas overlapping the Búði moraine, 10.2 ka), sealed by the Þorsá Lava (8.6 ka). (C) Synsedimentary micro-involutions due to tremors (Kelvin–Helmholtz convolutions) in early Holocene tidal rhythmites (ca. 9.6 ka). (D) Earthquake-graded gravel in a raised beach, close to Bitra (SISZ), south of Lake Hestvan (ca. 9.6 ka). (E) Offset accommodation of a tillite (11.4 ka BP) versus glaciofluvial sediments in a small graben located on a SISZ fault, Akbraut. Thick line, fault; thin line, glaciotectonic feature.

noted that the traces of paleo-earthquake ruptures are located in the southern prolongation of the Minnivellir–Skardsfjall fault system (earthquake of 1630; Einarsson and Eiriksson, 1982; Einarsson et al., 2002; Bergerat et al., 2011; Fig. 1C). The rupture observed in lower Member D (Fig. 7C and D) occurred on the same system, but at ca. 110 ka during the last unglaciated interval in the Rangá valley.

The first type is rather ubiquitous in deglaciation sedimentary facies, together with fault offsets in the sediments

https://doi.org/10.1017/qua.2019.68 Published online by Cambridge University Press

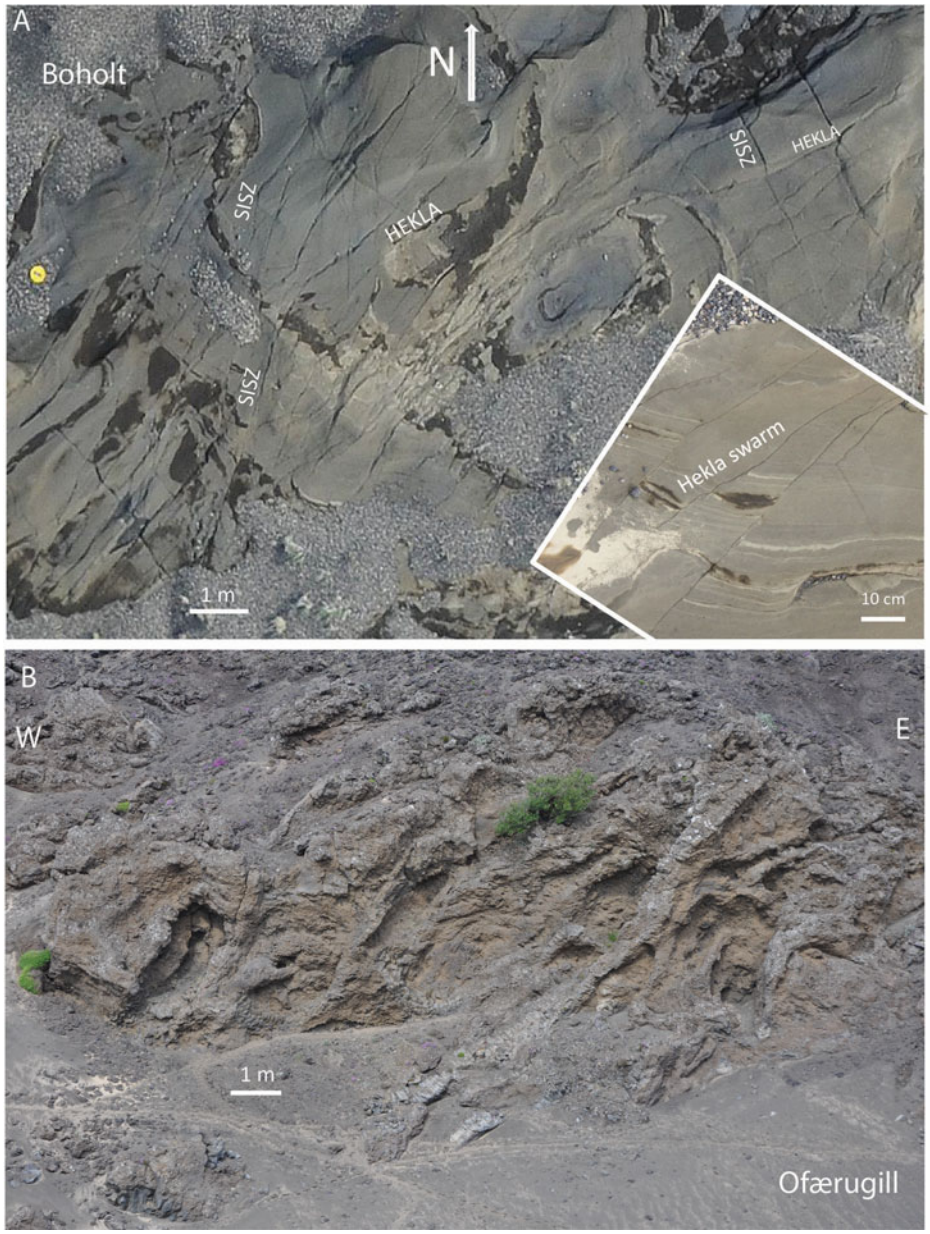

Figure 5. Fault systems in the Rangávellir. (A) Unit C2. UVA-generated orthophotograph showing the net of strike faults. The Hekla system is N45° to N60°. The SISZ is more variable in direction, including N45° and N155° fractures, but the main faults trend N10°. Typical trends are indicated here as "SISZ" and "HEKLA." The detailed picture is located 100 m to the right of the main view. Here, the faulting also affected Unit C3b. (B) Normal feed dykes of the Hekla fault system below a pillow lava accumulation, at the base of the Stöng sequence (Unit B1).

(Figs. 3, 5, and 6, Table 2 in the Supplementary Material) as commonly observed in western Europe and Alaska (Sauber and Molnia., 2004; Hampel et al., 2009; Brandes and Winsemann 2013). The second is commonly observed near known Holocene SISZ faults during full interglacial intervals (Fig. 4).

Fault activity (Rangá Formation)

Significant tectonic activity occurred during the progressive inundation of the Ytrí Rangá valley (Units C1 and C2; Fig. 5), in connection with low-magnitude earthquakes. There are two major sets of fractures—N40° to N70°, belonging to the Hekla system and being more scattered, and N170° to N210°, related to the SISZ. The fault set that follows the Hekla system is limited to the eastern side of the paleo-estuary (Fig. 2B). In the Rangá Formation, this fault set is associated with eruptions of the Hekla system with an early Plinian one (pumice and base surge in upper C2 unit, Supplementary Material) or basaltic tephra and the dated lava flow at Galtalækur (C3 unit). It also seems to support rapid unloading-related dyke injection in a subglacial position (Johnston, 1989; Stewart et al., 2000), as with the older pillow lava close to the base of the Stöng and Ofærugill sequences

https://doi.org/10.1017/qua.2019.68 Published online by Cambridge University Press

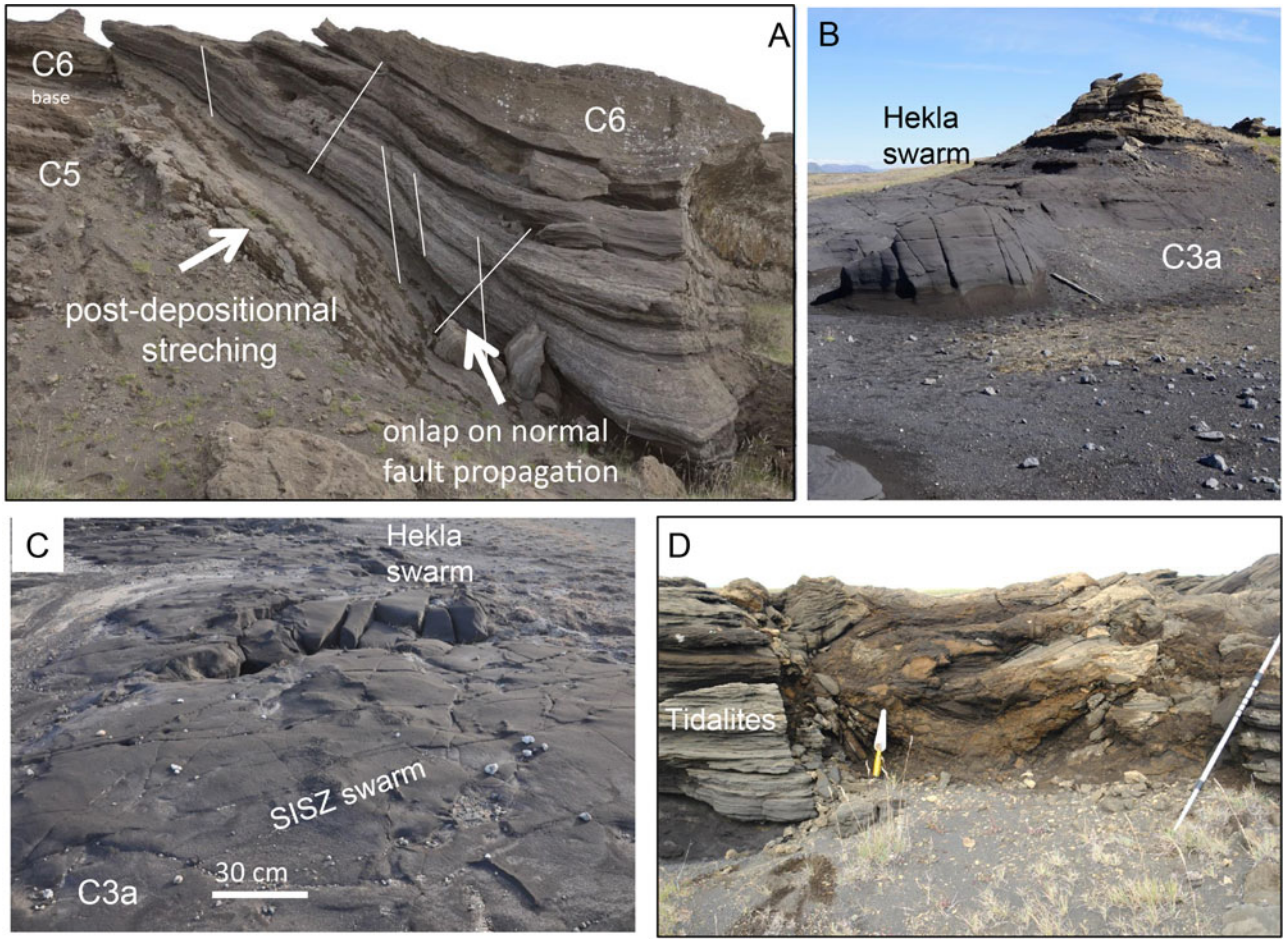

Figure 6. (color online) Fault activity at Heiðarbrekka West. (A) Synsedimentary rollover on a N48° trending fault of the Hekla system. (B) Same structure observed to the north. (C) Crossing of the SISZ and Hekla fractures. (D) Superficial evidence of rupture in Unit C4, SISZ-trending fractures sealed by Units C5 and C6.

(base of Unit B2; Fig. 5B). Renewed, slow fault activity, accommodated by a tidal rhythmite, seems to have been synchronous with the second inundation (Unit C6 at Heiðarbrekka, maximum flooding surface 2; Fig. 2) and was related to a temporary full deglaciation close to 116 ka, probably at altitude (>500 m asl), on the Hekla fault system (Figs. 1C and 6). Similarly, during the early Holocene at Akbraut, SISZ fault activity is recorded as a metric offset, deforming glaciofluvial deposits. This is associated with recurrent low-magnitude seismicity, further accommodated by an early tillite from an 11.4 cal ka glacial advance (Fig. 4E) deforming a Bárðarbunga tephra estimated at ca.11.35 cal ka (Lind and Wastergård, 2011).

West of the SISZ—Kleifarvatn and the hyaloclastite ridge of Hellutindar

Kleifarvatn is presently a lake, located in a N30°- and N90°-controlled graben, with its western side occupied by a complex hyaloclastite ridge. N–S-striking faults have been observed at several locations on the Reykjanes Peninsula (Guðmundsson, 1987; Clifton et al., 2003). Kleifarvatn corresponds with the connection between the SISZ and the Reykjanes Peninsula, west of Hengill Volcano (Fig. 2). This sequence has not yet been described. The base of the hyaloclastite ridge of Hellutindar (Fig. 8B) seems monophasic to the northeast, in the quarry at the foot of the Háuhnúkar Tindar (ridge prolongation; Fig. 1C, Supplementary Material), represented by an accumulation of slightly stratified, nonvesicular pillow lava (>40 m high; Fig. 8C). A late graben, with a complex morainic infill, longitudinally deforms this accumulation (Fig. 8D). Stratified hyaloclastites, tuffs, and, very locally, lapilli facies dominate toward the southwest. All these surfaces are glacially abraded. Several SISZ faults cross the ridge in narrow grabens, especially near the north coast of the Innristapi Peninsula, (Fig. 8D, Supplementary Material). Similar fault directions exist in the lake (Friðriksson, 2014), associated with a N–S sublacustrine ridge and hot springs (Fig. 8A), also seen north of Krisuvík. It should be noted that this N–S ridge is composed of pillow lava, is connected to the main hyaloclastite ridge (Friðriksson, 2014; Fig. 8A), and lacks traces of glacial erosion. Some dark dismantled lava crops out at the top of Hellutindar ridge (Fig. 8E, black).

The sedimentary sequence crops out on the Syðristapi (165 m asl) and Innristapi Peninsulas (210 m asl) in direct

https://doi.org/10.1017/qua.2019.68 Published online by Cambridge University Press

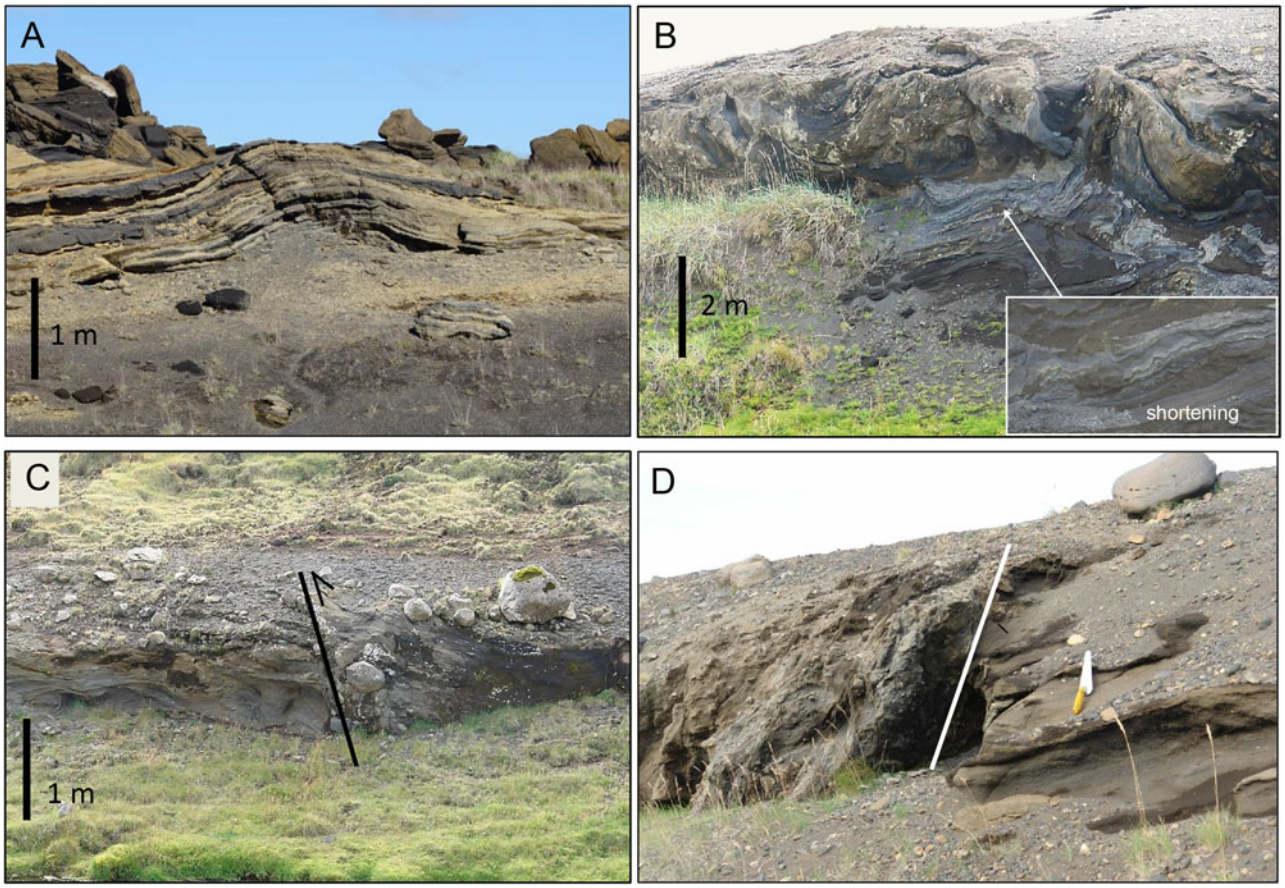

Figure 7. (color online) Faulting, folding, and synsedimentary loading, Rangávellir. (A) Heiðrabrekka West, local synsedimentary compressive structure (SISZ), sealed by unit C5. (B) Kirkjubær, Unit C3a, mega loadcasts with shortening figures. (C, D) Heiðrabrekka East, faulted units from the base of Member D in the SISZ system, cropping out in the Vikinglækur River, sealed by intact till (Member E), older than the Preboreal terminal moraine at ca.150 m north of the faults.

continuity of the last deposits of the hyaloclastite ridge. It is not possible to define precise units, because the facies is rather similar from the base to the top of the sequence. The lower unit—Unit A—consists of hyaloclastite deposits, washed downslope and faulted, on the Innristapi Peninsula (165 m asl; Figs. 8B and 9), attesting to an early collapse of the Kleifarvatn graben, scoured by a stratified till. It seems to correspond to a first transgression, associated with a deglaciation. It is covered by a local, thick basaltic tephra (lapilli) and is overlapped unconformably by later terrace sand deposits. These peninsulas are both covered by two sets of marine or lacustrine deposits that are devoid of bioturbation. Unit B, above Syðristapi, rests unconformably on the hyaloclastites at ca. 210 m asl and appears to be mostly subaquatic, exhibiting a few dropstones, water-escape features (Fig. 9), and reworked encapsulated tephra pellets (phreatomagmatic activity on the ridge). It probably signifies a highstand. The latest unit—Unit C (165 m asl)—is simpler and better stratified, with only limited small-convoluted bedding, and rests unconformably on Unit A. It signals a second highstand. It is further strongly faulted in the N30° and N90° directions. This water-lain formation mainly formed raised coastal ridges at 165 and 200 m asl (Supplementary Material) in the vicinity of the present-day coastline. It was strongly consolidated, latterly reddened, and deformed by a listric strike collapse toward the present lake. The lower level in altitude (Unit C) is much less developed, but forms a flat terrace at 165 m asl, also latterly reddened. The entrance to the graben at Krýsuvík is marked by a wide, perched marine abrasion surface at 80–110 m asl, supporting the old, abraded Selalda volcanic cones (reactivated during Termination Ib (Sæmundsson et al., 2016), armored by N120° dykes, and also rubified. The sequence at Kleifarvatn was further faulted by glaciotectonics and incised by meltwater channels.

The Hellutindar laminated hyaloclastite ridge was dated at 155 ± 58 ka (MIS 6b deglaciation age) based on a subglacial laminated hyaloclastite interstratified with basaltic sills (Sample ISLN-109; Table 3, Supplementary material) and signifies an ice margin position (Smellie, 2008). Its prolongation to the northeast, the Háuhnúkar Tindar ridge, is deformed as a graben with a complex morainic infill probably of MIS 6a age, further glacially abraded. This infill as also the subaerial sedimentary sequence of Kleifarvatn may thus be attributed to an interglacial period younger than the MIS 6a, but prior to the last glacial period (late-glacial abrasion). It thus records the MIS 5e interglaciation and yields a similar history to those observed in the central embayment (Table 1). Major faulting on the Innristappi Peninsula, following the

https://doi.org/10.1017/qua.2019.68 Published online by Cambridge University Press

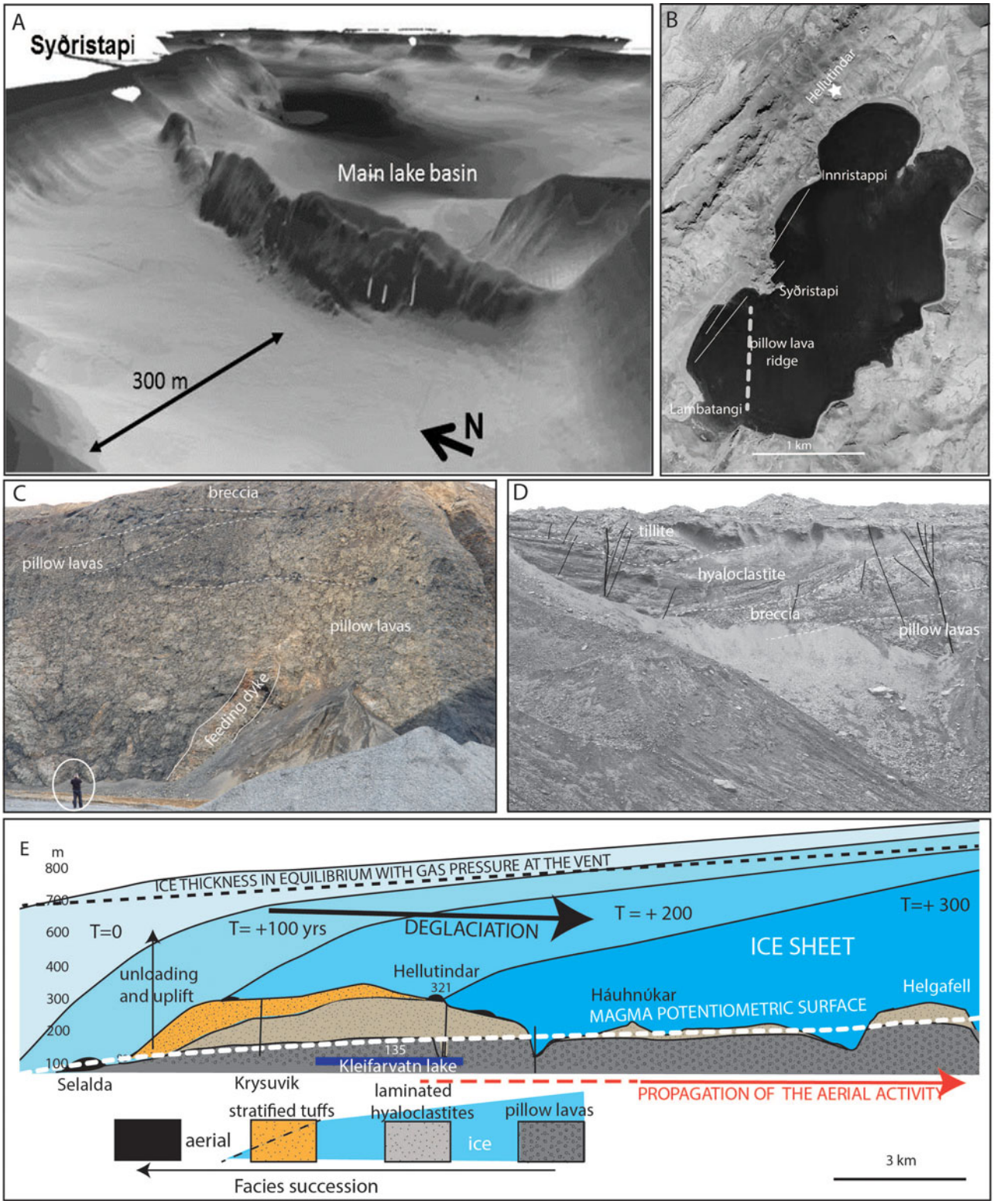

Figure 8. (color online) Kleifarvatn volcanic ridge record. (A, B) Pillow lava ridge, 800 m long, extending along a N–S fissure, south of Syðristapi (multibeam DEM, modified after Friðriksson, 2014, Figure 24, exaggerated twice in altitude; global picture from Lanmælingar Island). Pillow lavas also crop out at the southern extremity of the lake, at Lambatangi, with both N90° and N30° fractures; they are glacially abraded. (C) Pillow lava accumulation with feed dyke in the same hyaloclastite ridge, Háuhnúkar Quarry. (D) Longitudinal graben in the same hyaloclastite ridge, Háuhnúkar Quarry, filled by faulted tillite. (E) Sketch of deglaciation of the Hellutidar–Helgafell ridge, with basal pillow lava, laminated hyaloclastites to the south, and tuff accumulation, in early deglaciated zones (the time scale is hypothetical). Black bodies are postglacial basaltic scoria splays (Eemian?).

https://doi.org/10.1017/qua.2019.68 Published online by Cambridge University Press

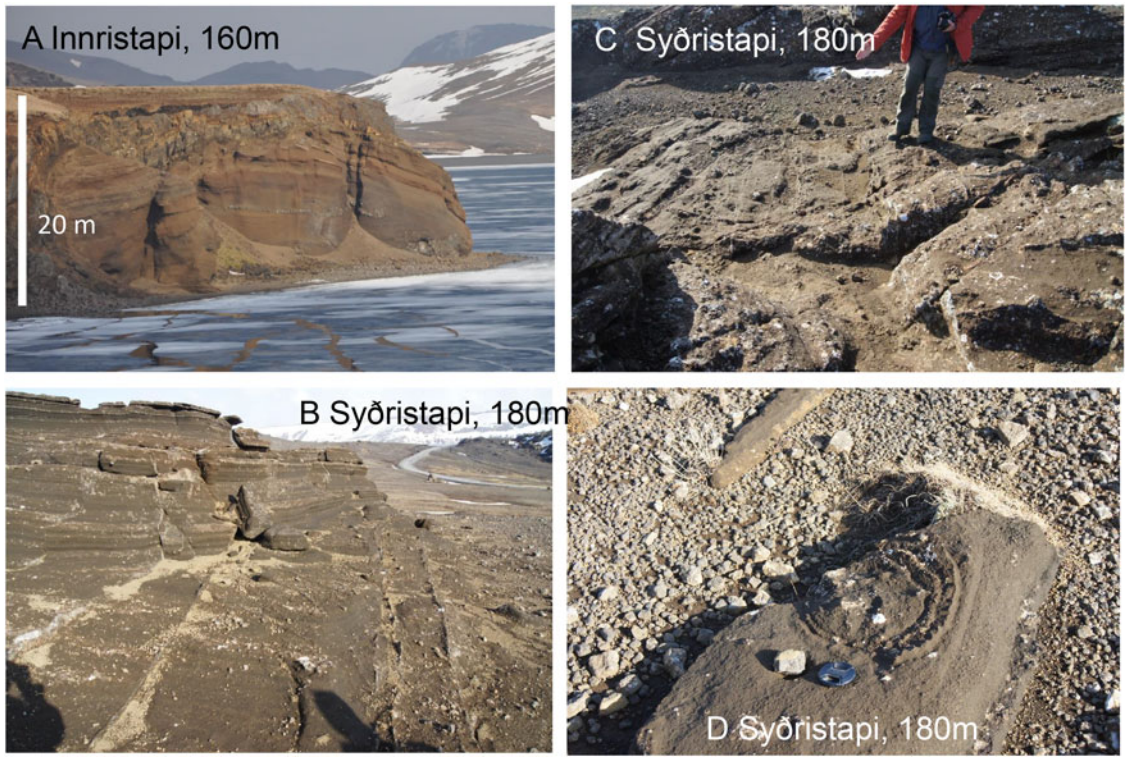

Figure 9. (color online) Kleifarvatn graben sedimentary record. (A) View of the Innristappi Peninsula, showing the strike-faulted Rangá Formation (lower unit of the formation; section ca. 17 m high, summit 160 m asl). (B, C) Two sets of faulting on the Syðristapi Peninsula (180 m asl), Unit B. (D) Horizontal cross-cutting of a water escape in Unit B. Glacial erosion was significant during the last deglaciation.

Reykjanes fault system, most likely records the 155–145 ka deglaciation (MIS 6b), similar to the Ófærugill record at the foot of the Hekla Volcano (Van Vliet-Lanoë et al., 2018). During the MIS 5e, Kleifarvatn formed a narrow bay that opened to the ocean during the deglaciation, with a relative sea level close to 210 m asl, probably corresponding to the level of MIS 5e Transgression I, with some volcanic activity on the ridge (lapilli), as recorded in Ytri–Rangá (215 m asl), and associated with marked faulting following both the SISZ and Reykjanes Peninsula trends. The second highstand is not well represented by sediments at 165 m asl (coastal ridges on an abrasion surface), due to the morphology of the bay (no fluvioglacial input), but the formation of the large tidal flat, close to 80–110 m asl, at the entrance to the bay at Krýsuvík (Fig. 2) attests to a progressive lowering of sea level between the two highstands, or, latterly, during the onset of the last glaciation.

DISCUSSION

Our observations have defined the first relative chronological record for all of the seismic and tectonic activity detected during several deglaciations in southern Iceland (Fig. 2, Table 1) in connection with the setting of tephras, lavas, and hyaloclastites ridges.

The knowledge of the stress state is important to distinguish faulting induced by glacial unloading (e.g., Wu and Hasegawa, 1996; Lund, 2005; Connor et al., 2009), often pasted with silty coatings, as opposed to pure tectonic activity. In Iceland, the stress state, controlled first by both plate divergence and volcanism, without glaciers, is responsible for the SISZ fault zone. The magma in Iceland is mostly supplied by the hot spot and the oceanic ridge, independent of glacial activity. The extension of the fault system seems to have been essentially controlled by magmatic overpressure, and commonly induced swell and fracture/dyke propagation and dyke intrusions appear to reduce the accumulated strain energy and bring the state of stress close to lithostatic (Guðmundsson, 2000). It resulted in the emplacement of significant subglacial volcanic products related to the supplementary melting in the upper mantle, such as tuyas and hyaloclastite ridges at the outer margins of the ice sheet, on reactivated rifts. Moreover, the ice cap also interacts as a confining system (Edwards et al., 2015). This should be especially true during a full glaciation, with the subglacial and subaerial lava emissions being emitted to the ice-sheet margins. This emission was prolonged during deglaciation by a remaining flat potentiometric surface.

Volcanism

The difference in height of the subglacial volcanoes or tuyas above the Icelandic plateau is considered to reflect a normal decrease in Pleistocene ice thickness toward the coast (Walker, 1965; Licciardi et al., 2007); however, it can also

https://doi.org/10.1017/qua.2019.68 Published online by Cambridge University Press

Table 1. Timing of the tectonic and seismic activity on the southern Icelandic embayment.

Member	Unit	Facies	RSL Ytri Rangá/Kleifavatnr	Estimated age G: Greenland stage/interstade	Period	Jökulhlaup[a]	Co-seismic[b]
F		Dunes		AD 1000	Holocene	++	Rupture
		Loesses	0	<8500 cal BP			No data
E		Tills + estuarian/deglacial	90		Late-glacial period to Preboreal	+++	Co-seismic
D	D2	Tills	?		Weichselian	?	
	D1	Glaciofluvial	?	<109 ka ca. GS 23	MIS 5c-5b		Rupture
C	C6 sup	Deglacial glaciofluvial (Hellar Cave tephra) Aeolian and colluvial	?	110–109 ka GI 23 (GS 24)	MIS 5d-5c	+	
	C6 low	Deglacial mudflat + loess	168/165	ca. 116–113 ka GI 25	MIS 5e	+++	Fault system
	C5	Loesses	0–20	ca. 120–116 ka GS 26		(+)	
	C4	Mudflat	215/210	ca. 126–120 ka		(+)	Rupture
	C3	Estuarian	140	ca. 127–126 ka		(+)	Co-seismic fault system
	C2	Estuarian	100	ca. 129–127 ka		++	Co-seismic fault system
	C1	Lacustrine and /fluviatile	?	ca. 132–129 ka		+++	Co-seismic fault system
B	−B3	Till + lacustrine/deglacial	?	ca. 140–132 ka	MIS 6a	+++	Co-seismic
	B2c	Lacustrine/till		ca. 150–140 ka	MIS 6b	++	—
	B2b	Slurry flow + lacustrine/deglacial	?	ca. 155–150 ka		+++	Fault system
	B1	Tills	?		MIS 6c		
A		Tills	?				

[a] The number of + indicates the relative frequency of jökulhlaups.
[b] Rupture: fault with offset recorded in stratigraphy and morphology; co-seismic: any kind of co-seismic features.

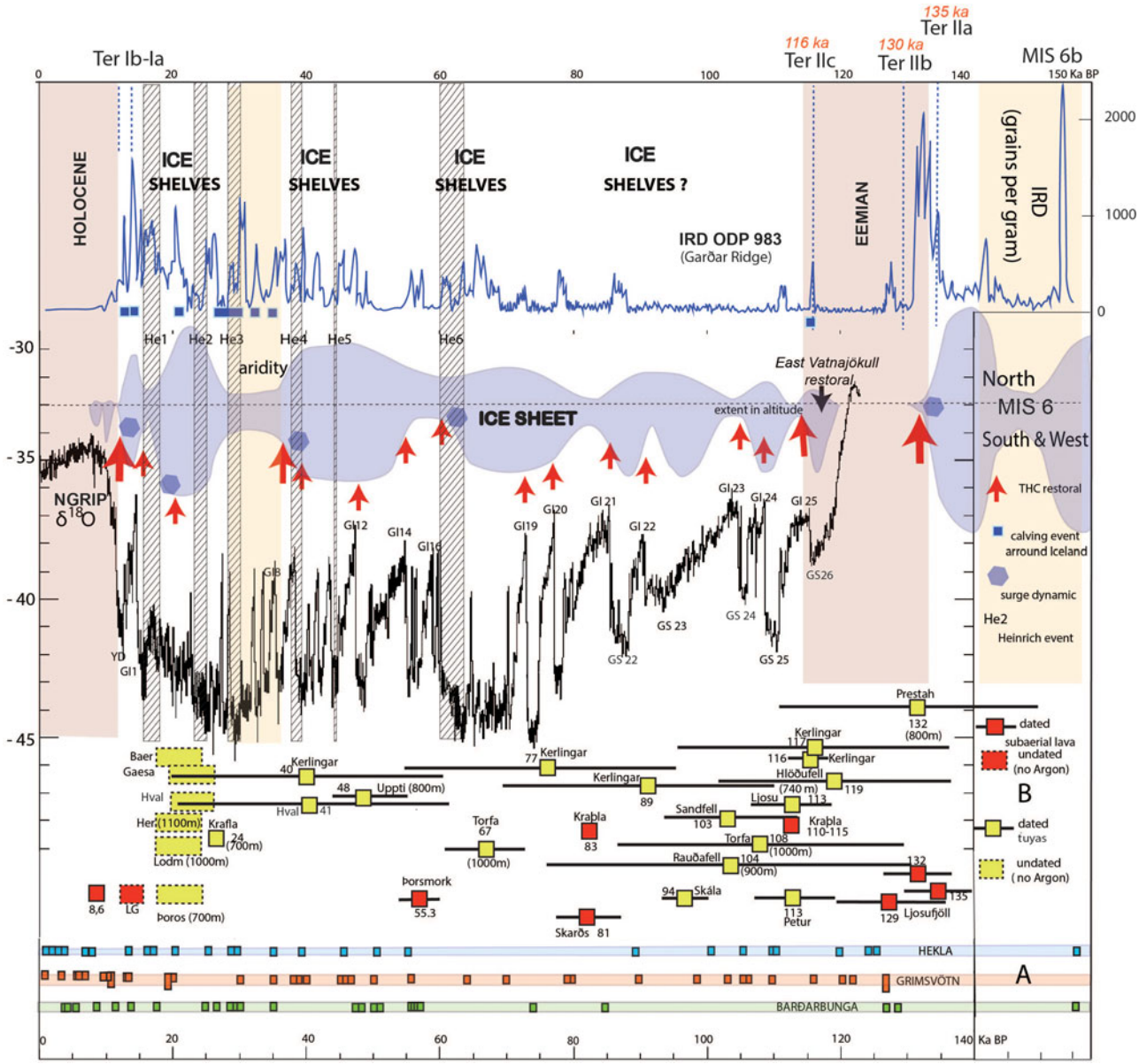

Figure 10. (color online) Stratigraphical and chronological relationships between volcanic activity (tephra, ridges and tuyas) and climate. NGRIP $\delta^{18}O$ curve (Andersen et al., 2004). Calving events and thermohaline circulation restoration after Rassmusen et al. (2016). Numbers between brackets correspond to estimated ice thickness on each tuya. Dating of tuyas shown in Table 1. Tephra: Oladottir et al. (2011), Davies et al. (2014), Voelker and Haflidason (2015), Van Vliet-Lanoë et al. (2018). Ocean Drilling Program 983 IRD record after Barker et al. (2015).

be considered to be a measure of the slope of the associated potential that over millennia (timing in ka), drove magma from the hot spot along the volcanic zones to the SISZ (Guðmundsson, 2000). Iceland is thus responding, in part, to the increased production of magma and its hydration (Wylie et al., 1999), as well as the propagation over centuries of fluidized magma limited to the already/recently unloaded zones (Eason et al., 2015).

During MIS 5, Grímsvötn seems to have been the most active and deglaciation-sensitive volcano (Van Vliet-Lanoë et al., 2018), probably in reaction to the location of its upper magmatic chamber (3 km) and its recurrent feeding by dykes issuing from the hot spot (Guðmundsson, 2000). This was also true during the Holocene (Óladóttir et al., 2011) and the entire last glaciation (Davies et al., 2014; Voelker and Haflidason, 2015; Fig. 10). The thick phreatomagmatic Grímsvötn 5e-low/BAS tephra of Unit C3 in its combination of successive eruptions presents a volume and a setting similar in timing to the complex Holocene Saksunarvatn tephra (see "Main Volcanic Systems"). This could signal the full entrance of the volcano into an interglacial regime. To control Grímsvötn's eruption susceptibility, we also analyzed past eruptive activity in the studied and adjacent volcanic zones. In the Ytrí Rangá valley, Member B (Unit B2) was emplaced during the penultimate glaciation (MIS 6; Fig. 10). The significant loading during this major glaciation

https://doi.org/10.1017/qua.2019.68 Published online by Cambridge University Press

apparently caused the Hekla fault system controlling the volcanic zone to become enlarged (Bourgeois et al., 1998), extending to the Norðubjallar ridge, 4 km distant from the main eruptive fissure, or even to Stöng (10 km; Figs. 1B and 5). Similarly, the early Plinian eruption of the Hekla occurred close to 129–128 ka (Fig. 3), after the deglaciation of Termination IIb and an early sagging of the estuary.

A similar situation was highly probable during the deglaciation event close to 155 ka (MIS 6b), when subglacial lava flows issued from Veiðivötn fault system (Fig. 1) and reached at least the Búrfell in the Ytri Rangá valley to become subaerial (Littlalækur; Table 1). The setting of the Unit B2a volcaniclastic deposits represents an intra-MIS 6b eruption of the Hekla Volcano at about the same age. This suggests synchronous major subglacial fissural activity in the entire EVZ (Fig. 1B). The early lapilli deposit at Inristappi yielded a similar signature for the WVZ. Other ridges were probably also synchronously active to the east (Fig. 1B), the south, and the west on the Reykjanes Peninsula (ca. 155 ka; Fig. 1B and C, Table 1). Their peculiar preservation is probably linked to the rapid glacial re-extension from 145 ka (MIS 6a). This volcanic activity on these enlarged subglacial ridges led to the emplacement of large volumes of hyaloclastite-derived sediments, located along the fault system during the MIS 6 deglaciation (Member C; Units C1 to C3). The record from ice and marine-sediment cores has not previously provided such evidence for a tephra emission from Grímsvötn Volcano at that time, but has well favoured a massive exportation of hyaloclastites-derived sediments (Bout-Roumazeilles et al., 1997).

Buildup and decay of the Icelandic ice sheet

The buildup of the Icelandic ice sheet was quite discrete in terms of timing, being under the control of available precipitation (Broecker and Denton, 1990). Its thickness was modulated by warming events or by precipitation starvation. It was favored by higher precipitation to the south and west, with a low snowline (Ahlmann and Þorarrinsson, 1937), as shown by the early MIS 5e development of the Mýrdalsjökull and Langjökull glaciers (Van Vliet-Lanoë et al., 2018). The northeast was more arid than today with a raised snowline (Hanna et al., 2004), thus relatively starving the development of the ice cap. During cooling events, the glacial dynamics seem to have been cold-based, with steep borders. During warming events, precipitation rose and glaciers evolved into polythermal or maritime types, with much more gradual slopes (Kerr, 1993). These warming events were driven by DO events (Rasmussen et al., 2016). Consequently, interstadial events raised the plasticity of the ice and increased sliding, favoring surging (Pattyn, 2003), ice shelf building, and glacial thinning. DO events resulted in rather continuous calving, with IRD recorded around Iceland (Fig. 10), especially from 40 ka (Jennings et al., 2000; van Kreveld et al., 2000; Geirsdottir et al., 2002; Bauch and Erlenkeuser, 2008; Barker et al., 2015; Fig. 10). Surging is common during melting events, especially in temperate-based or polythermal Arctic glaciers (Fowler et al., 2001; Sevestre et al., 2015), due to gravitational spreading of the inland ice sheet with the development of tidal calving and ice-stream thinning (Fig. 10). A volcanogenic water supply may have also helped the surging (Björnsson, 2009).

To evaluate the thickness of the ice sheet, we compared the altitudes of the tuya plateaus (Walker, 1965) with their topographical heights, arbitrarily adding a supplementary 400 m, which corresponds to the present-day ice thickness on the Grímsvötn volcanic caldera (Björnsson, 2009). This value is a minimum that could have been significantly greater, but still less than twice as thick from inland field data (nunataks, dated tuyas), with the exception of the thicker and more extended MIS 6, 10, 12, and 16 ice sheets. MIS 6 ice sheets were usually very thick and extended in the Northern Hemisphere (Svendsen et al., 2004; Lang and Wolf, 2011), as well as in Iceland (Van Vliet-Lanoë et al., 2005; Geirsdóttir et al., 2009), fitting the 1500–2000 m requirements used for models (e.g., Patton et al., 2017). In the south, such an average ice thickness was quite regular over the last glacial period, being between 800 and 1000 m (Fig. 10), much thinner than the 1500–2000 m used in models of massive "Weichselian inlandsis," speculated on offshore undated terminal moraines (e.g., Ingólfsson et al., 2010; Patton et al., 2017). This has been confirmed by the analysis of pressure-sensitive gas inclusions in quenched basalts by Tuffen et al. (2010) and volcaniclastic subglacial facies.

Glacioisostatic pressure, rebound, and seismic activity

The seismic activity in the SISZ during the Holocene was mostly related to plate-pull, accommodated by volcanic activity shear stress (Guðmundsson, 2000; Guðmundsson, 2006). The current seismic strain release in Iceland is controlled by rifting and by glacial loading and unloading (Sauber and Monia, 2004). As the lithosphere deforms, the downbending depending primarily on the extent, the area covered by the ice sheet (Guðmundsson, 1999) under control by the viscosity of the mantle, and the regional ice-loading history (Cuffey and Paterson, 2010). During interstadials and deglaciations, the SISZ reacted differently, as a significant amount of the shear stress (differential uplift and plate-pull) was compensated for by the injection of magma into dykes (Guðmundsson, 2000) and fault offsets. Presently, uplift related to the rapid deglaciation caused by modern global warming has reached ca. 2 cm/yr for the Vatnajökull ice sheet (Sigmundsson et al., 2010). Faster rates (6.9 to 8.2–10.5 cm/yr) have been estimated for Termination Ib in southern Iceland (Ingólfsson et al., 1995; Biessy et al., 2008).

Two types of paleoseismic records exist in the SISZ region. The first is associated with sediments offset by faults (abrupt or progressive) and recurrent low-Ms seismicity during the deposition of units the deglaciation of MIS 6b and ca. 129–127 ka (final MIS 5e deglaciation) of the Ytri–Rangá long sequence. This supports rapid unloading events, with active volcanism and dyke injection (Johnston, 1989; Stewart

https://doi.org/10.1017/qua.2019.68 Published online by Cambridge University Press

et al., 2000) along the Hekla fault system and also along the N–S faults of the SISZ (at Kleifarvatn). This is also the case for the last deglaciation (12–10.3 ka), as recorded at Akbraut (Fig. 4) and in northern Iceland (15–10.3 ka; Van Vliet-Lanoë et al., 2005) and for recent global warming (Bergerat and Angelier, 2003; Lindman et al., 2010) in the vicinity of Vatnajökull. Moreover, these events are often associated, based on the stratigraphy, with evidence of jökulhlaups (Table 1), a phenomenon commonly triggered by subglacial eruptions related to deglaciation (Björnsson, 2002, 2009).

The second type, corresponding to large interglacial earthquakes, is mostly recorded in the Ytrí Rangá valley during the end of the first transgression, in association with true ruptures in the SISZ, volcanic eruptions related to a rapid hydrostatic unloading downstream (onset of the first regression), and rapid glacial loading on the mountains (cooling GS26).

It should be noted that traces of paleo-earthquake ruptures are located in the southern prolongation of the Minnivellir–Skarðsfjall fault system, which has been activated several times historically (Einarsson et al., 2002; Bergerat and Angelier, 2003; Bergerat et al., 1998; Bergerat et al., 2011). The type and size of the co-seismic features suggest events of Mw > 6 (Obermeier et al., 1993; Olson et al., 2005) as was also the case in the early Holocene, as evidenced by the massive graded gravels in a raised beach at Þjoðolfshag (SISZ, Fig. 6D) following the experiments of Lagerbäck and Sundh (2008).

Deglaciation microseismicity

Large glacial loads generally suppress earthquakes, but conversely, rapid deglaciation promotes earthquakes in freshly deglaciated zones (Johnston, 1989; Hasegawa and Basham, 1989), as seen in Greenland today (Olivieri and Spada, 2015). In Iceland, seismicity is complicated by volcanism and the possibility of dyke injection. Low-level seismicity has been systemic in Iceland during deglacial events, whatever their significance, usually associated with dyke injection in northern Iceland (Einarsson and Brandsdottir, 1980; Van Vliet-Lanoë et al., 2005). Dyke intrusions along the Hekla or Kleifarvatn systems seem to have lowered the accumulated strain under deglacial conditions, especially close to the margins of the melting ice sheet. This is also valid for interglacial aftershocks that temporarily raise the water table and increase microseismicity (Saar and Manga, 2003; Jónsson et al., 2003; Decriem et al., 2010).

As explained earlier, the Termination IIb continental deglaciation (130–129 ka) proceeded faster than Termination Ib (11.7 ka). This explains the presence of lacustrine facies (Units B3 and C1) before marine flooding, with sea-level rise beginning around 135 ka (Termination IIa; Siddal et al., 2006; Fig. 10). Termination Ia (14.5 ka; Bölling Interstadial) and the MIS 6b long interstadial (155–145 ka; Ofærugill sedimentary record) evolved similarly. Because MIS 6 resulted in a relatively very large ice sheet, deglaciation rapidly moved landward with sagging, as proven by the progressive extent of the Rangá paleoestuary to the northeast (Van Vliet-Lanoe et al., 2018).

Deglaciation faulting

Increased pore pressure during deglaciation tends to weaken fault stability (Sigmundsson, 2006; Lund and Näslund, 2009), with the greatest effects at the end of glaciation due to a greater available water supply. On the other hand, rapid ongoing marine transgressions are responsible for hydrostatic loading on the formerly emerged platform, allowing relatively very fast flooding of the isostatically depressed zone. Loading may have increased N45° tension features along the Hekla fault system, and widening it by dyke injection, generating hyaloclastite ridges. To this day, these faults guide the superficial fluvial drainage (see Supplementary Material) and are frequently armored with dykes along the northwestern flank of the ridge. Moreover, this fault system represents evidence of an en échelon functioning (Allemand et al., 1989) of the Hekla system, in agreement with the thin and brittle character of the regional crust (Einarsson et al., 2006). If this system has been active since ca. 417 ka (dated feldspar from the ISLN112 Hekla pumice; Van Vliet-Lanoe et al., 2018), then this would imply an offset of 0.25 mm/yr, restricted to deglaciation periods only, with the displacement possibly reaching ca. 10 m by the end of the deglaciation event (over 1 ka). The observed vertical offset in Unit C6 at Heiðarbrekka is of this order of magnitude (4 m).

Evidence on the western side of the Hekla fault system suggests that rifting events occurred during at least two deglaciations—the early MIS 6b deglaciation and the MIS 6a/MIS5e—such as at Ofærugill (Unit B2) and with the Plinian eruption close to 128 ka. These events resulted in sagging, in the form of a hemi-graben, toward the embayment (Fig. 1C). This partly explains the preferential preservation of the interglacial formation on this side of the embayment. It probably also occurred during Termination Ib, enabling the flow of lava (Þjórsá Lava) and jökuhlaup along the eastern coast of the embayment, excavating the Rangá valley. This arrangement in asymmetric grabens has also been observed in Holocene formations of the Bárðarbunga–Veiðivötn system (Fig. 1B), and seems to be a classic feature of the Holocene volcanic systems of the EVZ, with fault offsets ranging between 4 and 22 m (Plateaux, 2012). To the west, along Kleifarvatn, fault-offset strikes follow the Reykjanes fault system (Clifton and Kattenhorn, 2006).

Large interglacial earthquakes in the Ytri Ranga valley

Glacial unloading temporarily modified the stress field, allowing the opening of fractures in the SISZ and South Volcanic Zone during interglaciations. During the onset of the last Bárðarbungá eruption (Guðmundsson et al., 2014), fissure opening was initially accompanied by a left-lateral shear that ceased with increased opening and magma injection. In the Northern Volcanic Zone (Jökulsà à Fjöllum valley), fissure opening occurred with the deposition of MIS

https://doi.org/10.1017/qua.2019.68 Published online by Cambridge University Press

5e deglacial sediments (Van Vliet-Lanoë et al., 1995), before the settling of the Grímsvötn 5e-Low/BAS IV tephra (ca. 127 ka; Van Vliet-Lanoë et al., 2018), and ended in the Mófell sector (north of Krafla Volcano), with lava fountains and spatter cones occurring inside the fissures.

The earthquake evidenced in synchronicity with the first MIS 5e regression in the YtrÍ Rangá valley (ca. 126–125 ka) was related to a rapid hydrostatic unloading downstream and to a rapid glacial loading upstream and associated with true ruptures in the SISZ (Fig. 6D) and also with eruptions in the Hekla system (Fig. 3). The accumulation of an extension deficit—responsible for large Holocene earthquakes—seems to have been primarily related to low water table levels in the eastern part of the SISZ during the drained full interglaciation, and secondarily to limited volcanic activity (dyke injection) in the west, the EVZ still being regularly active. Guðmundsson (2000) proposed that the Laki eruption in 1783 induced one of the largest historical earthquake in Iceland in 1784 (estimated magnitude 7.1). Because fluid injections (magma or water) into fissures are much less available during full interglaciations, it seems logical that the extension deficit would increase at that time. This could also be the case for early interstadials (MIS 5d, low water table) in regions with a delayed glaciation.

Most of the other factures are arranged en échelon, with the N–S orientation typical of the SISZ, organized in several fault arrays (e.g., Sigmundsson et al., 1995; Einarsson et al., 2002; Bergerat et al., 2011; Angelier et al., 2004). They are influenced by preexisting fractures (Ruch et al., 2016), re-using faults activated during the MIS 5e and probably earlier. These were probably initiated during the first stage of the development of the SISZ, as shown by fractures that occur outside the present range of the SISZ, north of the Búrfell (Fig. 1C), at large angles to the main left-lateral shear and displaying an opposing sense of motion (i.e., right-lateral displacement; e.g., Bergerat and Angelier, 2008). Fracturing could also have allowed for a rapid breaking of the tectonic displacements, and thus a change in earthquake type, through rapid drainage of the upper crust, similar to the drainage that occurred at Kleifarvatn after the 2000 earthquake (Clifton et al., 2003).

Subglacial volcanism

Magma and water potentials

The observed recurrent microseismicity seems to be related in time to upper mantle decompression, with a deglaciation-forced basal reservoir and dyke injection along existing volcanic systems (Guðmundsson, 2000; Hartley and Thordarson, 2013), not only with the thickness of the ice sheet as commonly stressed (Walker, 1965; Licciardi et al., 1997). As inferred by numerical models by Andrew and Guðmundsson (2007), the pressure on the magma reservoirs increases under glacial load, and so does the melt temperature, meaning there is less melt available under the glacial load (glacial periods) than during melting periods (early interglacial periods).

With a maximal ice load (ca. 1500 m of ice at the LGM), a crustal deflection of 500 m inland would be expected for a mean plateau altitude of around 600 m. Downbending generates horizontal compressive stress, which can stop dyke injections and inhibit eruptions (Guðmundsson, 1986, 1999; Andrew and Guðmundsson, 2007; Sinton et al., 2005; Sigmundsson et al., 2010; Eason et al., 2015). The present surface of the basaltic basement below the ice sheet will evolve into a flat or down-warped subglacial topography.

Downbending also implies a minimal magma overpressure to produce lava eruption, with the potentiometric surface being very low angled, making for easier dyke injection and eruption in zones where the ice load is less significant, such as at the margins of the ice cap (Fig. 8E) or at the thinned head of an ice stream. Moreover, due to unloading, the melting glacial margins will experience the largest stress increase (Pagli and Sigmundsson, 2008), with emission of extensive aerial lava flows (Guðmundsson, 1986, 2000) extending outside the ice sheet, often in the form of lava shield. In this case, the slope of the magma potential is much more important compared with major deglacial times, and probably a limited production of mantle melting would be enough to produce large lava splay, as at Holuhraun in 2014 or in the Ytrí Rangá in the early MIS 5e.

Furthermore, during early deglaciation, the isostasy-forced flat topography simultaneously aided in the formation of large, subglacial aquifers or event lakes at the ice-sheet base. It enhanced the effects of earthquakes (Sibson, 1994; Mulargia and Bizzarri, 2014), and finally provoked basal sliding of the ice sheet, promoting glacial surges and accelerating glacial thinning.

Tuya and hyaloclastite ridge formation

Magma supply is key to all subglacial injections, shutting down once its pressure falls below the glaciostatic pressure (Smellie and Skilling, 1994; Smellie, 2008). Guðmundsson (2011a, 2011b) demonstrated that magma emergence is related to a complex combination of overpressure of the magma in the dykes, magma and crustal densities and effects of layering in the crust. Tuya and hyaloclastite ridges should develop under glaciers with an ice thickness being assumed to be sufficient (>500 m) to restrict volcanic explosivity to phreatomagmatic processes (Guðmundsson et al., 2004; Höskuldsson et al., 2006; Smellie, 2006; Edwards et al., 2015), allowing the construction of a subaqueous tuff cone superimposed on the pillow lava volcano (Smellie, 2000; Tuffen et al., 2010; Edwards et al., 2015). This is observed in the southwestern part of the hyaloclastite ridge of Hellutindar. Conversely, the common basal accumulation of non-vesiculated pillow lava—the first step in building tuyas or ridges—is a result of high cooling rates from water at hydrostatic pressures of more than 600–700 m (Jones, 1969; Aumento, 1971; Zimbelman and Gregg, 2000; Russell et al., 2014), as in the Háuhnúkar Tindar, north of Kleifarvatn. The preliminary construction phase of the Hlöðufell tuya (240 m thick; Skilling, 2009) would have required a

https://doi.org/10.1017/qua.2019.68 Published online by Cambridge University Press

pressure equivalent to 740 m of ice thickness. These values are in agreement with a thinned ice sheet and some melting.

The ridges seem also to be predominantly related to greater magma injection than the tuyas, feeding on a preexisting wide volcanic system containing tension fractures, normal faults, and dykes (Guðmundsson, 2000; Hartley and Thordarson, 2013; Rubin and Gillard, 1998), as seen at Kleifarvatn, supplied by the Mid-Atlantic Ridge (Höskuldsson et al., 2007). Another system for ridge formation is likely magma injection mostly fed by a large, elongated reservoir at the base of the crust (Hartley and Thordarson, 2013; Guðmundsson et al., 2014), rather than by a chamber, because fissure eruptions result from subvertical dykes rupturing the surface during rifting events and may occur close to or independent of the central volcano. This would explain the volume of such ridge emplacement during relatively brief rifting events, unlocked by glacial unloading and melting production at the base of the crust and, following our observation, near the ice-sheet margin (Fig. 8E). For tuyas, the homogeneity of their geochemistry suggests these are chamber-fed features (Eason et al., 2015), probably initially driven by deeper, large, elongated reservoirs at the base of the crust (Hartley and Thordarson, 2013). Their formation is thus less sensitive to major unloading than the ridges, but could be more sensitive to local unloading.

Volcaniclastic interstratified tuff and basalt facies are good indicators of full or limited deglaciation episodes (Smellie, 2008), although ice thickness cannot be precisely constrained based on this lithofacies (Lachowycz et al., 2015). In the absence of dating, the development of hyaloclastite/pillow lava ridges has been considered to have mostly occurred around the time of the LGM at the ice divide (Carrivick et al., 2009; Bourgeois et al., 1998), but also during the deglaciation, especially tuya (cf. Licciardi et al., 2007). From our data, tuyas and hyaloclastite ridges (Fig. 10; other ridges of southern Iceland, Supplementary Material, p. 12) seem mostly to have formed during MIS 6b and correspond to transitional periods during buildup phases of the ice sheet, temporary melting phases in interstadials, or even during full deglaciations.

Dating of tuyas and hyaloclastite ridges

As mantle production and hot-spot activity pre-dated the glaciation, they have certainly interfered with the impact of a full or a limited deglacial unloading and the chain of interactions that this has induced. The K–Ar ages obtained from the Hlöðufell and Rauðafell tuyas (Table 3, Supplementary material) are significantly older than the He-exposure ages obtained by Licciardi et al. (2007) and Eason et al. (2015).

Minor amounts of unresolved excess ^{40}Ar can significantly bias K–Ar ages obtained from samples containing very small amounts of radiogenic Ar, as is the case in the K–Ar-dated samples from the Hlöðufell and Rauðafell tuyas and as discussed in Guillou et al. (2019). Such excess Ar could explain the differences between the K–Ar and He-exposure ages. An alternative explanation is that the tuyas might be polygenic. Indeed, a single tuya may erupt several times during a single glaciation, such as the Snæfell (Höskuldsson and Imsland, 1998; Guillou et al., 2010). More recent tuya eruptions, such as the upper Herðubreið (Werner et al., 1996), seem to correspond to the late reactivation of an older tuya related to the Herðubreiðtögl tuya (256 ± 66 ka; Guillou et al., 2010) and are clearly multiphasic. Eason et al. (2015) considered that most of the tuyas they investigated were monogenic, on the basis of uniformity in geochemical composition alone, which is insufficient evidence to support such a view. Step-like platforms on tuyas can also be formed by successive lava-fed hyaloclastite deltas (Smellie et al., 2006). The dating of different units in a single tuya is crucial, but has yet to be done.

Plotting the ages of the subglacial activity from K–Ar dating (Table 3 Supplementary material) over the last 150 ka (Fig. 10), it appears, on the surface, that tuyas and hyaloclastite ridges mostly formed during ice-sheet buildup/loading phases that increased the primary mechanical vertical stress ($\sigma 1$; Fig. 10), especially during the early glacial stages, but also blocked the dyke propagation. A more detailed analysis, however, indicates that volcanic activity occurred during both the interglaciations and the glaciations (Guillou et al., 2010). The high frequency of formation of tuyas and hyaloclastite ridges seems to have occurred at least twice—during the early glacial time, probably linked with large interstadials, and after the Ålesund interstadial (35–27 ka). This most likely resulted from rapid variations in ice thickness, as unloading events triggered by melting intervals such as DO events (Fig. 10) probably temporarily destabilized the magmatic chamber(s) (Höskuldsson et al., 2006), although the ca. 10% accuracy of the K–Ar dating with low potassium content does not allow for a more precise chronology at this point, especially for the upper last glacial period. Relatively brief interstadial deglaciation events lasting for less than 5 ka during a period of ice-sheet reconstruction could also, and more logically, drive the formation of subglacial volcanoes (Fig. 10). A rapid ice-melt thinning of 100 m per century could be expected for DO events, given the present melting rate of the Vatnajökull, estimated at ca. 1 m/yr (https://www.glacierguides.is/vatnajokull-general-information, November 2018). Another thinning is expected from ice-stream formation, as presently seen on Victoria Land (Antarctica).

The MIS 6c glacial stage was cold and wet, and thus susceptible to the accumulation of a relatively very thick ice sheet, more significant than that of the previous glaciation (Fig. 10). Unloading, particularly during the MIS 6b interstadial (155–145 ka), was significant enough to generate ridges on the Kleifarvatn and Veiðivötn fault systems but also at the ridge of Kárahnjúkar (Sandfell) with emersion of the ice sheet (Jökuldalsheiði, west of Halslón lake; Table 3, Supplementary material). It is possible that the outer ridges of the Kverkfjöll, analyzed by Carrivick et al. (2009), also correspond to MIS 6b, as these ridges crop at the same distance of the Vatna magma feeding sources, with limited reactivation during Termination I. The small Skarðsengi ridge in the North Volcanic Zone (northeastern Iceland) is more

https://doi.org/10.1017/qua.2019.68 Published online by Cambridge University Press

recent, but is also related to a limited deglaciation (80 ka, MIS 5a interstadial; Guillou et al., 2010). A computer-generated map of the Vatnajökull subglacial topography (Björnsson, 2009) shows that many fewer ridges formed during the final deglaciation than in the Younger Dryas stadial at the terrestrial margins of the Weichselian ice sheet.

Tephra and glaciation

The drainage of a subglacial volcanic lake can further (re)activate explosive eruptions by lowering the pressure on the magma chamber (Höskuldsson et al., 2006; Albino et al., 2010; Smellie, 2010). Tephra-emitting eruptions at Grímsvötn Volcano (Davies et al., 2014; Voelker and Haflidason, 2015) occurred relatively constantly throughout the last glaciation, were relatively irregular in the Veiðivötn-Bárðarbunga volcanic system, were more clustered at Hekla Volcano, and were apparently rare during the period of maximal ice-sheet load (Fig. 10).

Concerning Bárðarbunga, the tephra signal is quite clear, in relation to a 12-km-deep magmatic chamber. Activity was, based on the entire available tephra record (Holocene to early MIS 5e; Davies et al., 2014; Voelker and Haflidason, 2015; Guðmundsdóttir et al., 2016; Van Vliet-Lanoë et al., 2018), limited during the MIS 5e, but persistent during the Weichselian and late-glacial times, probably due to a straightforward connection to a deep, large subcrustal reservoir. Activity was sustained during the major DO events, from 62 to 48 ka (Fig. 10), specifically the MIS 3 warmings and Heinrich event (HE) 6 (Marshall et al., 2006), just before a period of ice-cap thickening. The warmings were responsible for a thinning of the ice sheet, probably resulting from the development of ice streams (enhanced ice plasticity), as observed today in Antarctica (Rignot et al., 2008), and calving, as proven by recorded IRD (Fig. 10). The present position of this volcano, on the western side of Vatnajökull, seems very susceptible to ice thinning, as has been seen recently. A second peak of activity developed from 35 to 27 ka in connection with HE 4 and a warming equating to the Ålesund interstadial (Norway; Mangerud et al., 1981). The final activity began ca. 18 ka, ending with Termination Ib, including HE 1 and the major warming of the Bölling interstadial (Fig. 10).

The Hekla volcanic system appears to have expanded during Termination IIb. This enabled volcanic activity to occur with early rhyolitic pyroclastic flows, ca. 129–128 ka, at the C2/C3 unit boundary, apparently at the onset of glacial thinning in the southern embayment and basaltic eruption close to the thermal optimum at ca. 127–126 ka, during the deposition of Units C4 and C5 (Galtalækur lava flow, 2 tephra; Fig. 3), synchronous with the end of a rapid glacio-isostatic rebound and with activity associated with the SISZ, as is discussed for the Holocene by Guðmundsson and Brenner (2003). Following this, the activity became more episodic, even nonexistent, from 90 to 55 ka—the main period of ice-cap thickening with limited IRD production (Fig. 10). Similar to Bárðarbunga, activity at Hekla increased from MIS 3, after HE 6, persisting until Termination I (Fig. 10). Activity became quite regular due to Hekla's emergence, probably as a result of a thinning of the glacier via the ice streams that occupied the southern embayment. This volcano definitively pierced the ice sheet from ca. 55 ka, producing a good record of tephra emissions. As it is a fissure stratovolcano, a direct link to a subcrustal melt, driven by unloading, can be proposed from 55 ka. The Þórsmörk valley, north of the Myrdaljökull glacier, was also ice-free when thick tephra fell at ca. 55 ka (Torfjökull Volcano; Moles et al., 2019). Today, Hekla Volcano reaches 1488 m asl, 400–500 m higher than the surrounding tuyas, and thus probably emerged to ca. 300 m above the maximal ice thickness (900 m) after 55 ka. It is logical, using these results, to propose an early collapse, by surging, of the southern Icelandic ice sheet from the H6 event. The marine core record from the Gardar Ridge, southwest of Iceland, shows a massive input of IRD and ashes from 48 ka (Ash Zone II; Haflidalson et al., 2000).

CONCLUSIONS

In southern Iceland, late-glacial deposits and lava flows, the MIS 5e interglacial stage, and the Ófærugill/Hellutindar deglaciation event attest to six main unloading phases (MIS 6b, Terminations IIa, IIb, and IIc and Ia and Ib; Fig. 10). All of these were associated with synsedimentary seismic activity of low intensity, usually linked to dykes, ice-edge hyaloclastite ridge, and perhaps tuya injection. The occurrence of intrusive and extrusive volcanic activity during glacial unloading seems to have occurred commonly in association with dynamic extension, uppermost mantle decompression, magmatic fracturing, and volcanism. Glacial unloading seems to be the major trigger for surface geodynamics in glaciated volcanic provinces, even though surface geodynamics is primarily the triggered by deeper, mantle-driven rifting events, independent of glaciations. Also, high water levels, as commonly occur during deglaciations and maximal inundations (early interglaciations) likely eased the rifting by lowering the shear resistance close to the surface. From the record in the Ytrí Rangá long sequence, fault offsets in the WVZ and EVZ were more likely linked to deglacial unloading alone, unlocking local volcanic activity, even during short-lived events.

Evidence for a higher frequency of large earthquakes was not found in relation to deglaciation events, such as during the early MIS 5e and the Greenland interstadial GIS 25. Higher-magnitude seismic events appear to be linked to active N–S segments of the SISZ that also reactivated during the Holocene, and triggered by stress disequilibrium related to regional volcanic activity and drained conditions in the upper crust.

From the tephrostratigraphic records of marine and ice cores, the activity of the Grímsvötn Volcano seems to have been quite constant since MIS 5e. Fissure system activity seems to have been controlled by glacial unloading, with fault system enlargement favored by fracture opening related to unlocked rifting and major dyke injection. The activity of

https://doi.org/10.1017/qua.2019.68 Published online by Cambridge University Press

Hekla Volcano seems to have been sporadic since the middle Pleistocene. Fissural volcanic activity in the Bárðarbunga–Veiðivötn system was similar, but more constrained by the glacial unloading of the volcanic system.

ACKNOWLEDGMENTS

This study was funded by the French Polar Institute Paul-Emile Victor (IPEV), Arctic Research Program no. 316 (ICPROCI I, II, and III), and in part by the 4th and 5th programs of the European Union (PRENLAB 1 and 2, PREPARED) for fieldwork in Iceland. We especially thank Kristjan Sæmundsson for providing the original dating for the Krafla caldera. We also thank Audrey Wayolle and Guillaume Gosselin for their assistance during fieldwork in 2006 and 2008. This paper has benefited from helpful reviews and comments by Agust Guðmundsson (Royal Holloway), Kelly Russell, and an anonymous reviewer and from the editorial suggestions of N. Lancaster and J. Urrutia Fucugauchi.

SUPPLEMENTARY MATERIAL

The supplementary material for this article can be found at https://doi.org/10.1017/qua.2019.68

REFERENCES

Ahlmann, H.W., Þorarrinsson, S., 1937. Vatnajökull: Scientific results of the Swedish-Icelandic investigations. *Geografyska Annaler* 19, 176–231.

Albino, F., Pinel, V., Sigmundsson, F. 2010.Influence of surface load variations on eruption likelihood: application to two Icelandic subglacial volcanoes, Grímsvötn and Katla. *Geophysical Journal International* 181:1510–1524.

Allemand, P., Brun, J.P., Davy, P., Van Den Driessche, J., 1989. Symétrie et asymétrie des rifts et mécanismes d'amincissement de la lithosphère. *Bulletin de la SocIété Géologique de France* 8, 445–451.

Andersen, K.K., North GRIP Members, 2004. High resolution climate record of the Northern Hemisphere reaching into the last Interglacial Period. *Nature*. 2004 Sep 9; 431(7005):147–51. doi:10.103/nature02805.

Andrew, R.E.B., Guðmundsson, A., 2007. Distribution, structure and formation of Holocene lava shield in Iceland. *Journal of Volcanology and Geothermal Research*, 168, 137–154.

Angelier, J., Bergerat, F., 2002. Behaviour of a rupture of the 21 June earthquake in South Iceland as revealed in an asphalted car park. *Journal of Structural. Geology* 24, 1925–1936.

Angelier, J., Bergerat, F., Bellou, M., Homberg, C., 2004. Co-seismic strike-slip displacement determined from push-up structures: the Selsund Fault case, South Iceland. *Journal of Structural Geology* 26, 709–724.

Aumento, F., 1971, Vesicularity of mid-ocean pillow lavas. *Canadian Journal of Earth Sciences* 8, 1316–1319.

Auriac, A., Sigmundsson, F., Hooper, A., Spaans, K.H., Björnsson, H., Pálsson, F., Pinel, V., Feig, K.L., 2014. InSAR observations and models of crustal deformation due to a glacial surge in Iceland. *Geophysical Journal International* 198, 1329–1341.

Barker, S., Chen, J., Gong, X., Jonkers, L., Knorr, G., Thornalley, D., 2015. Icebergs not the trigger for North Atlantic cold events. *Nature Geoscience* 520, 333–336.

Bauch, H., & Erlenkeuser, H. 2008. A "critical" climatic evaluation of last interglacial (MIS 5e) records from the Norwegian Sea. *Polar Research*, 27(2), 135–151.

Bergerat, F., Angelier, J., 2003. Mechanical behavior of the Árnes and Hestfjall Faults of the June 2000 earthquakes in Southern Iceland: inferences from surface traces and tectonic model. *Journal of Structural Geology* 25, 1507–1523.

Bergerat, F., Angelier, J., 2008. Immature and mature transform zones near a hot spot: the South Iceland Seismic Zone and the Tjörnes Fracture Zone (Iceland). *Tectonophysics* 447, 142–154.

Bergerat, F., Angelier, J., Guðmundsson, Á., Torfason, H., 2003. Push-ups, fracture patterns, and paleoseismology of the Leirubakki Fault, South Iceland. *Journal of Structural Geology* 25, 591–609.

Bergerat, F., Guðmundsson, Á., Angelier, J., Rögnvaldsson, S.Th., 1998. Seismotectonics of the central part of the South Iceland Seismic Zone. *Tectonophysics* 298, 319–335.

Bergerat, F., Homberg, C., Angelier, J., Bellou, M., 2011. Surface traces of the Minnivellir. Réttarnes and Tjörvafit seismic faults in the South Iceland Seismic Zone: Segmentation, lengths and magnitude of related earthquakes. *Tectonophysics* 498: 11–26.

Bergerat, F., Plateaux, R., 2012. Architecture and development of (Pliocene to Holocene) faults and fissures in the East Volcanic Zone of Iceland. *Comptes-Rendus Geoscience* 344, 191–204.

Biessy, G., Dauteuil, O., Van Vliet-Lanoë, B., Wayolle, A., 2008. Fast and partitioned post-glacial rebound of south-western Iceland. *Tectonics* 27, TC3002.

Björnsson, H., 1998 Hydrological characteristic of the drainage system beneath a surging glacier. *Nature* 395, 771–774.

Björnsson, H., 2002. Subglacial lakes and jökulhlaups in Iceland. *Global and Planetary Change* 35, 255–271.

Björnsson, H., 2009. *Jöklar á Íslandi*. Bókaútgáfan Opna, Reykjavík. Translated into English as *The Glaciers of Iceland*. Atlantis Advances in Quaternary Science 2. Atlantis Press/Springer (2017). Amsterdam.

Björnsson, H., Pálsson, F., Sigurðsson, O., Flowers, G.E., 2003. Surges of glaciers in Iceland. *Annals of Glaciology* 36, 82–90.

Bourgeois, O., Dauteuil, O., Van Vliet-Lanoë, B., 1998 Subglacial volcanism in Iceland: tectonic implications. *Earth and Planetary Sciences Letters* 164, 165–178.

Bout-Roumazeilles, V., Debrabant, P., Labeyrie, L., Chamley, H., Cortijo, E., 1997. Latitudinal control of astronomical forcing parameters on the high-resolution clay mineral distribution in the 45–60 ° N range in the North Atlantic Ocean during the past 300,000 years. *Paleoceanography*, 12, 5, 671–686.

Brandes, C., Winsemann, J., 2013. Soft sediment deformation structures in NW Germany caused by Late Pleistocene seismicity. *International Journal of Earth Sciences* 102, 2255–2274.

Broecker, W.S., Denton, G.H., 1990. The role of ocean-atmosphere reorganisation in glacial cycles. *Quaternary Science Reviews* 9, 305–341.

Carrivick, J.L., Russell, A.J., Rushmer, E.L., Tweed, F.S., Marren, P.M, Deeming, H., Lowe, O.J., 2009. Geomorphological evidence towards a de-glacial control on volcanism. *Earth Surface Processes and Landforms* 34, 1164–1178.

Clifton, A.E., Kattenhorn, S.A., 2006. Structural architecture of a highly oblique divergent plate boundary segment. *Tectonophysics* 419, 27–40.

Clifton, A.E., Pagli, C., Jónsdóttir, J.F., Eythórsdóttir, K., Vogfjörd, K., 2003. Surface effects of triggered fault slip on Reykjanes Peninsula, SW Iceland. *Tectonophysics* 369, 145–154.

Connor, C.B., Chapman, N.A., Connor, L.J., 2009. *Volcanic and Tectonic Hazard Assessment for Nuclear Facilities*. Cambridge University Press, Cambridge (UK).

Cotten, J., Le Dez, A., Bau, M., Caroff, M., Maury, R.C., Dulski, P., Brousse, R., 1995. Origin of anomalous rare-earth element and yttrium enrichments in sub aerially exposed basalts: evidence from French Polynesia. *Chemical Geology* 119, 115–138.

Cuffey, K.M., Paterson, W.S.B., 2010. *The Physics of Glaciers*. 4th ed. Academic Press. 704pp, Amsterdam.

Dahl-Jensen, D., NEEM community members. 2013. Eemian interglacial reconstructed from a Greenland folded ice core. *Nature* 493 (7433):459–60.

Davies, S.M., Abbott, P.M., Meara, R.H., Pearce, N.J.G., Austin, W.E.N., Chapman, M.R., Svensson, A., Bigler, M., Rasmussen, S.O., Farmer, E.J., 2014. A North Atlantic tephrostratigraphical framework for 130–60 ka b2k: new tephra discoveries, marine-based correlations, and future challenges. *Quaternary Science Reviews* 106, 101–121.

Decriem, J., Árnadóttir, T., Hooper, A., Geirsson, H., Sigmundsson, F., Keiding, M., Ófeigsson, B.G., Hreinsdóttir, S., Einarsson, P., LaFemina, P. and Bennett, R. A., 2010. The 2008 May 29 earthquake doublet in SW Iceland. *Geophysical Journal International* 181, 1128–1146.

Eason, D., Sinton, J. M., Grönvold, K., Kurz, M., 2015 Effects of deglaciation on the petrology and eruptive history of the Western Volcanic Zone, Iceland. *Bulletin of Volcanology* 77(6). http://dx.doi.org/10.1007/s00445-015-0916-0.

Edwards, B.R., Guðmundsson, M.T., Russell, J.K., 2015. Glaciovolcanism. In: Sigurdsson, H., Houghton, B., McNutt, S.R., Rymer, H., Stix, J. (Eds.), *Encyclopedia of Volcanoes*. 2nd ed. Elsevier Inc., pp. 377–393.

Einarsson, P., 1991. Earthquakes and present-day tectonism in Iceland. *Tectonophysics* 189, 261–279.

Einarsson, P., Böttger, M., Thorbjarnarson, S., 2002. *Faults and Fractures of the South Iceland Seismic Zone near Thjórsá*. Landsvirkjun Report LV-2002/090. Landsvirkjun, Reykjavik.

Einarsson, P., Brandsdottir, B., 1980. Seismological evidence for lateral magma intrusion during the July 1978 deflation of the Krafla Volcano in NE Iceland. *Journal of Geophysiscal Research* 47, 160–165.

Einarsson, P., Eiriksson, J., 1982. Earthquake fractures in the districts Land and Rangarvellir in the South Iceland Seismic Zone. *Jökull* 32, 113–120.

Einarsson, P., Khodayar, M., Clifton, A., Ófeigsson, B., Thorbjarnarson, S., Einarsson, B., Hjartardóttir, Á.R., 2005. A map of Holocene fault structures in the South Iceland Seismic Zone. *Geophysical Abstract Research*, 7, communication 08858.

Einarsson, T., 1994. *Geology of Iceland. Rock and Landscape*. Mal og menning, Reykjavík.

Etzelmüller, B., Farbrot, H., Guðmundsson, Á., Humlum, O., Tveito, O.E., Björnsson, H., 2007. The regional distribution of mountain permafrost in Iceland. *Permafrost and Periglacial Processes* 18, 185–199.

Flowers, G.E., Björnsson, H., Geirsdóttir, Á., Miller, G.H., Clarke, G.K.C., 2007. Glacier fluctuation and inferred climatology of Langjökull ice cap through the Little Ice Age. *Quaternary Science Reviews* 22, 2337–2353.

Flowers, G.E., Björnsson, H., Geirsdóttir, Á., Miller, G.H., Black, J.L., Clarke, G.K.C., 2008. Holocene climate conditions and glacier variation in central Iceland from physical modelling and empirical evidence. *Quaternary Science Reviews* 27, 797–813.

Fowler, A.C., Murray, T., Ng, F.S.L., 2001. Thermal regulation of glacier surging. *Journal of Glaciology* 47, 527–538.

Friðriksson, Á., 2014. *What Is below the Water Masses? Multibeam Studies of Öskjuvatn, Thingvallavatn and Kleifarvatn*. MSc thesis, Geology, University of Iceland, Reykjavík.

Geirsdóttir, Á., Andrews, J.T., Ólafsdóttir, S., Helgadóttir, G., Harðardóttir, J. 2002. A 36 Ky record of iceberg rafting and sedimentation from north-west Iceland. *Polar Research* 21, 291–298.

Geirsdottir, A., Eirıksson, J., 1994. Growth of an intermittent ice sheet in Iceland during the late Pliocene and early Pleistocene. *Quaternary Research*, 42, 115–130.

Geirsdóttir, Á., Hardardóttir, J., Sveinbjörnsdóttir, Á.E., 2000. Glacial extent and catastrophic meltwater events during the deglaciation of Southern Iceland. *Quaternary Science Reviews* 19, 1749–1761.

Geirsdóttir, Á., Miller, G.H., Andrews, J.T., 2007. Glaciation, erosion, and landscape evolution of Iceland. *Journal of Geodynamics* 43, 170–186.

Geirsdóttir, Á., Miller, G.H., Axford, Y., Ólafsdóttir, S., 2009. Holocene and latest Pleistocene climate and glacier fluctuations in Iceland. *Quaternary Science Reviews* 28, 2107–2118.

Guðmundsdóttir, E.R., Larsen, G., Björck, S., Ingólfsson, Ó., Striberger, J., 2016. A new high-resolution Holocene tephra stratigraphy in eastern Iceland: improving the Icelandic and North Atlantic tephrochronology. *Quaternary Science Reviews* 150, 234–249.

Guðmundsson, A., 1986. Mechanical aspects of postglacial volcanism and tectonics of the Reykjanes Peninsula, Southwest Iceland. *Journal of Geophysical Research* 91, 12711–12721.

Guðmundsson, A., 1987. Geometry, formation and development of tectonic fractures on the Reykjanes Peninsula, southwest Iceland. *Tectonophysics* 139, 295–308.

Guðmundsson, A., 1999, Postglacial crustal doming, stresses and fracture formation with application to Norway. *Tectonophysics* 307, 407–419.

Guðmundsson, A., 2000. Dynamics of volcanic systems in Iceland. Example of tectonism and volcanism at juxtaposed hot spot and mid-ocean ridge systems. *Annual Review of Earth and Planetary Sciences* 8, 107–140.

Guðmundsson, A., 2006, How local stresses control magma chamber ruptures, dyke injections, and eruptions in composite volcanoes. *Earth Sciences Reviews* 79, 1–31.

Guðmundsson, A., 2011a. Deflection of dykes into sills at discontinuities and magma-chamber formation. *Tectonophysics* 500, 50–64.

Guðmundsson, A., 2011b. *Rock Fractures in Geological Processes*. Cambridge University Press, Cambridge, UK.

Guðmundsson, A., 2017. *The Glorious Geology of Iceland's Golden Circle*. Springer Verlag. Berlin-Heidelberg (Germany).

Guðmundsson, A., Brenner, S.L., 2003. Loading of a seismic zone to failure deforms nearby volcanoes: a new earthquake precursor. *Terra Nova* 15, 187–193.

Guðmundsson, A., Lecoeur, N., Mohajeri, N., Thordarson, T., 2014. Dike emplacement at Bardarbunga, Iceland, induces unusual stress changes, caldera deformation, and earthquakes. *Bulletin of Volcanology* 76, 869.

Guðmundsson, M.T., Jónsdóttir, K., Hooper, A., Holohan, E., Halldórsson, S., Ófeigsson, B., Cesca, S., *et al.*, 2016. Gradual caldera collapse at Bárdarbunga volcano, Iceland, regulated by lateral magma outflow. *Science* 353(6296). http://dx.doi.org/10.1126/science.aaf8988.

Guillou, H., Scao, V., Nomade, S., Van Vliet-Lanoë, B., Liorzou, C., Guðmundsson, Á., 2019. 40Ar/39Ar dating of the

https://doi.org/10.1017/qua.2019.68 Published online by Cambridge University Press

Thorsmork ignimbrite and Icelandic sub-glacial rhyolites. *Quaternary Science Reviews* 209, 52–62.

Guillou, H., Van Vliet-Lanoë, B., Guðmundsson, Á., Nomade, S., 2010. New unspiked K–Ar ages of Quaternary sub-glacial and sub-aerial volcanic activity in Iceland. *Quaternary Geochronology* 5, 10–19.

Haflidason, H., Eiriksson, J., van Kreveld, S. 2000. The tephrochronology of Iceland and the North Atlantic region during the Middle and Late Quaternary: a review. *Journal of Quaternary Sciences* 15, 3–22.

Halldorsson, S.A., Oskarsson, N., Grönvold, K., Sigurdsson, G., Sverrisdóttir, G., Steinthorsson, S., 2008. Isotopic-heterogeneity of the Thjorsa lava—implications for mantle sources and crustal processes within the Eastern Rift Zone. Iceland. *Chemical Geology* 255, 305–316.

Hampel, A., Hetzel, R., Maniatis, G., Karow, T., 2009, Three-dimensional numerical modeling of slip rate variations on normal and thrust fault arrays during ice cap growth and melting. *Journal of Geophysical Research*, 114, B08406.

Hanna, E., Jonsson, T., Box, J.E., 2004. An analysis of Icelandic climate since the nineteenth century. *International Journal of Climatology* 24, 1193–1210.

Hartley, M. E., Thordarson, T., 2013. The 1874–1876 volcano-tectonic episode at Askja, North Iceland: lateral flow revisited. *Geochemistry, Geophysics, Geosystems* 14, 2286–2309.

Hasegawa, H.S., Basham, P., 1989. Spatial correlation between seismicity and postglacial rebound in eastern Canada. In: Gregerson, S., Basham, P. (Eds.), *Earthquakes at North-Atlantic Passive Margins: Neotectonics and Postglacial Rebound*. Kluwer, Dordrecht, Netherlands, pp. 483–500.

Heifetz, E., Agnon, A., Marco, S., 2005. Soft sediment deformation by Kelvin Helmholtz instability: a case from Dead Sea earthquakes. *Earth and Planetary Sciences Letters* 236, 497–504.

Hjaltadóttir, S., 2009. *Use of relatively located microearthquakes to map fault patterns and estimate the thickness of the brittle crust in Southwest Iceland*. Msc Thesis Geophysics, Reykjavík University, Iceland, 104 p.

Hjartarson, A., Ingólfsson, O., 1988. Preboreal glaciation of Southern Iceland. *Jökull* 38, 1–13.

Höskuldsson, Á., Hey, R., Kjartansson, E., Guðmundsson, G.B., 2007. The Reykjanes Ridge between 63°10′N and Iceland. *Journal of Geodynamics* 43, 73–86.

Höskuldsson, A., Imsland, P., 1998. Snaefell volcano in a future volcanic zone. [In Icelandic.] *Glettingur* 8, 22–30.

Höskuldsson, A., Sparks, R.S.J., Carroll, M.R., 2006. Constraints on the dynamics of subglacial basalt eruptions from geological and geochemical observations at Kverkfjöll, E-Iceland. *Bulletin of Volcanology* 68, 689–701.

Huybers, P. J., Langmuir, C. 2009. Feedback between deglaciation, volcanism, and atmospheric CO_2. *Earth and Planetary Sciences Letters* 286, 479–491.

Ingólfsson, Ó., 1991. A review of the Late Weichselian and early Holocene glacial and environmental history of Iceland. In: Maizels, J., Caseldine, C. (Eds.), *Environmental Change in Iceland: Past and Present*. Kluwer Academic, Dordrecht, Netherlands, pp. 13–29.

Ingólfsson, Ó., Norðdahl, H., Haflidason, H., 1995 Rapid isostatic rebound in southwestern Iceland at the end of the last glaciation. *Boreas* 24:245–259.

Ingólfsson, Ó., Norddahl, H., Schomaker, A., 2010. Deglaciation and Holocene glacial history of Iceland. *Development in Quaternary Sciences* 13:51–68.

Innocent, C., Fléhoc, C., Lemeille, F., 2005. U-Th vs. AMS 14C dating of shells from the Achenheim loess (Rhine Graben). *Bulletin de la Société Géologique de France* 176, 249–255.

Jackson, M.G., Oskarsson, N., Trønnes, R.G., McManus, J.F., Oppo, D.W., Grönvold, K., Hart, S.R., Sachs, J.P., 2005. Holocene loess deposition in Iceland: evidence for millennial scale atmosphere-ocean coupling in the North Atlantic. *Geology* 33, 509–512.

Jakobsdóttir, S.S., 2008. Seismicity in Iceland: 1994–2007. *Jökull* 58, 75–100.

Jennings, A., Syvitski, J., Gerson, L., Grönvold, K., Geirsdóttir, Á., Hardardóttir, J., Andrews, J., Hagen, S., 2000. Chronology and paleoenvironments during the late Weichselian deglaciation of the southwest Iceland shelf. *Boreas* 29, 163–183.

Johanesson, H. and Sædmundsson, K., 1998. *Geological map of Iceland, 1/500 000*, 2d edition, Icelandic Institute of Natural History, Reykjavík.

Johannesson, H., Sæmundsson, K., Jakobsson, S.P., 1990. Geological Map of Iceland. Sheet 6, South-Iceland. Museum of Natural History and the Iceland Geodetic Survey, Reykjavik.

Johannsdottir, G.E., 2007. Mid-Holocene to Late Glacial Tephrochronology in West Iceland as Revealed in Three Lacustrine Environments. MS thesis, University of Iceland, Reykjavík.

Johnston, A.C., 1989. The effect of large ice sheets on earthquake genesis. In: Gregerson, S., Basham, P.W. (Eds.), *Earthquakes at North-Atlantic Passive Margins: Neotectonics and Postglacial Rebound*. Kluwer Academic Pub, Dordrecht, pp. 581–599.

Jones, J. G., 1969. Pillow lavas as depth indicators. *American Journal of Science* 267, 181–195.

Jónsson, S., Segall, P., Pedersen, R., Björnsson, G., 2003. Post-earthquake ground movements correlated to pore-pressure transients. *Nature*, 424, 179–183.

Jull, M., McKenzie, D., 1996. The effect of deglaciation on mantle melting beneath Iceland. *Journal of Geophysical Research* 101, 815–821, 828.

Keeling, C.D., Whorf, T.P., 2000. The 1,800-year oceanic tidal cycle: a possible cause of rapid climate change. *Proceedings of the National Academy of Sciences USA* 97, 3814–3819.

Kerr, A., 1993. Topography, climate and ice masses: a review. T*erra Nova* 5, 332–342.

Kristjánsson, L., Duncan, R.A., Guðmundsson, Á., 1998. Stratigraphy, paleomagnetism and age of volcanics in the upper regions of Þjórsárdalur valley, central south Iceland. *Boreas* 27, 1–13.

Kutterolf, S., Jegen, M., Mitrovica, J.X., Kwasnitschka, T., Freundt, A., Huybers, P.J., *et al*., 2013. A detection of Milankovitch frequencies in global volcanic activity. *Geology* 41, 227–230.

Lachowycz, L.M., Pyle, D.M., Gilbert, J.S., Mather, T.M., Mee, K., Naranjo, J.A., Hobb, K.L., 2015. Glaciovolcanism at Volcán Sollipulli, southern Chile: lithofacies analysis and interpretation. *Journal of Volcanology and Geothermal Research* 303, 59–78.

Lagerbäck, R., Sundh, M., 2008. *Early Holocene Faulting and Paleoseismicity in Northern Sweden*. Research Paper C 836. Geological Survey of Sweden, Uppsala.

Lang, N., and E. W. Wolff, 2011: Interglacial and glacial variability from the last 800 ka in marine, ice and terrestrial archives. *Climate of the Past*, 7, 361–380.

Larsen, G., Eiríksson, J., Knudsen, K.L., Heinemeier, J., 2002. Correlation of late Holocene terrestrial and marine tephra markers in North Iceland: implications for reservoir age changes, *Polar Research*. 21, 283–290.

https://doi.org/10.1017/qua.2019.68 Published online by Cambridge University Press

Larsen, G., Guðmundsson, M.T., Björnsson, H., 1998. Eight centuries of periodic volcanism at the center of the Iceland hot spot revealed by glacier tephrastratigraphy. *Geology* 26, 943–946.

Li, Z.-X.A., Lee, C.-T.A., 2006. Geochemical investigation of serpentinized oceanic lithospheric mantle in the Feather River Ophiolite, California: implications for the recycling rate of water by subduction. *Chemical Geology* 235, 161–185.

Licciardi, J.M., Kurz, M.D., Curtice, J.M., 2007. Glacial and volcanic history of Icelandic table mountains from cosmogenic ^{3}He exposure ages. *Quaternary Science Reviews* 26, 1529–1546.

Lind, E., Wastegård, S., 2011. Tephra horizons contemporary with short early Holocene climate fluctuations: new results from the Faroe Islands. *Quaternary International* 246, 157–167.

Lindman, M., Lund, B., Roberts, R., 2010 Spatiotemporal characteristics of aftershock sequences in the South Iceland Seismic Zone: Interpretation in terms of pore pressure diffusion and poroelasticity. *Geophysical Journal International* 183(3):1104–1118. DOI: 10.1111/j.1365-246X.2010.04812.x

Lowe, D.R., LoPiccolo, R.D., 1974. The characteristics and origins of dish and pillar structures. *Journal of Sedimentary Petrology* 44, 484–501.

Lund, B., 2005. Large earthquakes during a glacial cycle. In: Hora, S., Jensen, M., *Expert Panel Elicitation of Seismicity following Glaciation in Sweden*. Report 2005:20. Swedish Radiation Protection Authority, Stockholm, Sweden, pp. 107–119.

Lund, B., Näslund, J.O., 2009. Glacial isostatic adjustment: implications for glacially induced faulting and nuclear waste repositories. In: Connor, C.B., Chapman, N.A., Connor, L.J. (Eds.), *Volcanic and Tectonic Hazard Assessment for Nuclear Facilities*. Cambridge University Press, chap. 10, pp. 142–155, Cambridge, (UK).

Maclennan, J., Jull, M., McKenzie, D., Slater, D., Grönvold, K., 2002. The link between volcanism and deglaciation in Iceland. *Geochemistry, Geophysics, Geosystems* 3:1062.

Mangerud, J., Gulliksen, S., Larsen, E., Longva, O., Miller, G.H., Sejrup, H.P., Senstegaard, E., 1981. A Middle Weichselian ice-free period in Western Norway: the Alesund Interstadial. *Boreas* 10:447–462.

Marshall, S.J., Koutnik, M.R., 2006. Ice sheet action versus reaction: distinguishing between Heinrich events and Dansgaard-Oeschger cycles in the North Atlantic. *Paleoceanography* 21, PA2021.

McManus, J.F., Oppo, D.W., Keigwin, L.D., Cullen, J.L., Bond, G.C., 2002. Thermohaline circulation and prolonged interglacial warmth in the North Atlantic. *Quaternary Research* 58, 17–21.

Millot, R., Guerrot, C., Innocent, C., Négrel, Ph., Sanjuan, B., 2011. Chemical, multi-isotopic (Li-B-Sr-U-H-O) and thermal characterization of Triassic formation waters from the Paris Basin. *Chemical Geology* 283, 226–241.

Minster, J.F., Ricard, L.P., Allègre, C.J., 1979. ^{87}Rb-^{87}Sr chronology of enstatite meteorites. *Earth and Planetary Science Letters* 44, 420–440.

Moles, J.D., McGarvie, D., Stevenson, J.A., Sherlock, S.C., Abbott, P.M., Jenner, F.E., Halton, A.M., *et al*., 2019. Widespread tephra dispersal and ignimbrite emplacement from a subglacial volcano (Torfajökull, Iceland). *Geology* 47, 577–580.

Mulargia, F., Bizzarri, A., 2014. *Anthropogenic triggering of large earthquakes. Scientific Reports* 4, 6100.

Obermeier, S.F., 1996. Using liquefaction induced features for paleoseismic analysis. In: McCalpin, J. (Ed.), *Paleoseismology*, pp. 331–396. Academic Press, Amsterdam.

Obermeier, S. F., Martin, J. R., Frankel, A. D., Youd, T. L., Munson, P. J., Munson, C.A., Pond, E. C., 1993. Liquefaction evidence for one or more strong Holocene earthquakes in Wabash Valley of southern Indiana and Illinois, with a preliminary estimate of magnitude: U.S. Geological Survey Professional Paper 1536, 27 p.

Óladóttir, B.A., Larsen, G., Sigmarsson, O., 2011. Holocene volcanic activity at Grímsvötn, Bárdarbunga and Kverkfjöll subglacial centres beneath Vatnajökull, Iceland. *Bulletin of Volcanology* 73, 1187–1208.

Olivieri, M., and Spada, G., 2015. Ice melting and earthquake suppression in Greenland. *Polar Science* 9, 94–106.

Olson, S., Green, R., Obermeier, S. F., 2005. Revised magnitude-bound relation for the Wabash Valley seismic zone of the Central United States. *Seismological Research Letters* 76, 756–771.

Owen, G., Moretti, M., Alfaro, P., 2011. Recognising triggers for soft-sediment deformation: current understanding and future directions. *Sedimentary Geology* 235, 133–140.

Pagli, C., Sigmundsson, F., 2008. Will present day glacier retreat increase volcanic activity? Stress induced by recent glacier retreat and its effect on magmatism at the Vatnajökull ice cap, Iceland. *Geophysical Research Letters* 35, L09304.

Plateaux, R. (2012). *Architecture et mécanismes du rift islandais dans la région du Vatnajökull*. PhD thesis, Nice-Sophia-Antipolis University, Nice, France.

Patton, H., Hubbard, A., Bradwell, T., Schomacker, A., 2017. The configuration, sensitivity and rapid retreat of the Late Weichselian Icelandic ice sheet. *Earth Science Reviews* 166, 223–245.

Pattyn, F., 2003. A new three-dimensional higher-order thermomechanical ice sheet model: basic sensitivity, ice stream development, and ice flow across subglacial lakes. *Journal of Geophysical Research, Solid Earth* 108, 2382.

Pierrot-Deseilligny, M., Paparoditis, N., 2006. A multiresolution and optimization-based image matching approach: an application to surface reconstruction from SPOT5-HRS stereo imagery. *International Archives in Photogrammetry and Remote Sensing* 36(1/W41).

Praetorius, S., Mix, A., Jensen, B., Froese, D., Milne, G., Wolhowe, M., Addison, J., Prahl, F., 2016. Interaction between climate, volcanism, and isostatic rebound in Southeast Alaska during the last deglaciation. *Earth and Planetary Sciences Letter*. 452, 79–89.

Principato, S.M., Moyer, A.N., Hampsch, A.G., Ipsen, H.A., 2016. Using GIS and streamlined landforms to interpret palaeo-ice flow in northern Iceland. *Boreas* 45, 470–482.

Rasmussen, T.L., Thomsen, E., Kuijpers, A., Wastegård, S., 2003. Late warming and early cooling of the sea surface in the Nordic seas during MIS 5e (Eemian Interglacial). *Quaternary Science Reviews* 22, 809–821.

Rasmussen, T.L., Thomsen, E., Moros, M., 2016. North Atlantic warming during Dansgaard-Oeschger events synchronous with Antarctic warming and out-of-phase with Greenland climate. *Nature Science Report* 6, 20535.

Rawson, H., Pyle, D.M., Mather, T.A., Smith, V.C., Fontijn, K., Lachowycz, S.M., Naranjo, J., 2016. The magmatic and eruptive response of arc volcanoes to deglaciation: insights from southern Chile. *Geology* 44, 251–254.

Reverso, T., Vandemeulebrouck, J., Jouanne, F., Pinel, V., Villemin, T., Sturkell, E., Bascou, P., 2014. A two-magma chamber model as a source of deformation at Grimsvötn Volcano, Iceland. *Journal of Geophysical Research* 119, 4666–4683.

Rignot, E., Bamber, J.L., Van Den Broeke, M.R., Davis, C., Li, Y., Van De Berg, W.J., Van Meijgaard, E., 2008. Recent Antarctic

ice mass loss from radar interferometry and regional climate modelling. *Nature Geoscience* 1, 106.

Rögnvaldsson, S.Th., Slunga, R., 1994. Single and joint fault plane solutions for microearthquakes in South Iceland. *Tectonophysics* 237, 73–80.

Rubin, A.M., Gillard, D., 1998. Dike-induced earthquakes: theoretical considerations. *Journal of Geophysical Research* 103, 10017–10030.

Ruch, J., Wang, T., Xu, W., Hensch, M., Jónsson, S., 2016. Oblique rift opening revealed by reoccurring magma injection in central Iceland. *Nature Communications* 7. doi:10.1038/ncomms1235.

Russell, J.K., Edwards, B.R., Porritt, L., Ryane, C., 2014. Tuyas: a descriptive genetic classification. *Quaternary Science Reviews* 87, 70–81.

Saar, M.O., Manga, M., 2003. Seismicity induced by seasonal groundwater recharge at Mt. Hood, Oregon. *Earth and Planetary Sciences Letters* 214, 605–618.

Sæmundsson, K., Sigurgeirsson, M.A., Hjartarson, A., Kaldal, I., Kristinsson, S.G., 2016. Geological Map of Southweast Iceland. 1:100 000. 2nd ed. Iceland Geosurvey, Reykjavík.

Sauber, J.M.and Molnia, B.F., 2004. Glacier ice mass fluctuations and fault instability in tectonically active southern Alaska. *Global and Planetary Change* 42, 279–293.

Seidenkrantz, M.S., Bormalm, L., Dansgaard, W., Johnsen, S.F., Knudsen, K.L., Kuijpers, A., Lauritzen, S.E., *et al*., 1996. Two-step deglaciation at the oxygen isotope stage 6/5e transition: the Zeifen-Kattetgat climatic oscillation. *Quaternary Science Reviews* 15, 63–75.

Sevestre, H., Benn, D.I., Hulton, N.R.J., Bælum, K., 2015. Thermal structure of Svalbard glaciers and implications for thermal switch models of glacier surging. *Journal of Geophysical Research, Earth Surface* 120, 2220–2236.

Sibson, RH., 1994. Crustal stress, faulting and fluid flow. In: Parnell, J. (Ed.), *Geofluids: Origin, Migration and Evolution of Fluids in Sedimentary Basins. Geological Society of London Special Publication* 78, 69–84.

Siddall, M., E. Bard, E. J. Rohling, and C. Hemleben (2006b), Sea-level reversal during T II, *Geology*, 34(10), 817–820, doi:10.1130/G22705.1.

Sigmundsson, F., Einarsson, P., Bilham, R., Sturkell, E., 1995. Rift-transform kinematics in south Iceland: deformation from Global Positioning System measurements, 1986–1992, *Journal of Geophysical Research*, 100, 6235–6248.

Sigmundsson, F., Pinel, V., Lund, B., Albino, F., Pagli, C., Geirsson, H., Sturkell, E. 2010.Climate effects on volcanism: influence on magmatic systems of loading and unloading from ice mass variations, with examples from Iceland368Philosophical Transactions of the Royal Society A: Mathematical, Physical and Engineering Sciences http://doi.org/10.1098/rsta.2010.0042

Sims, J.D., 1975. Determining earthquake recurrence intervals from deformational structures in young lacustrine sediments. *Tectonophysics* 29, 141–152.

Sinton, J., Grönvold, K., Sæmundsson, K., 2005, Postglacial eruptive history of the Western Volcanic Zone, Iceland. *Geochemistry, Geophysics, Geosystems* 6, Q12009.

Skilling, I.P. 2009. Subglacial to emergent basaltic volcanism at Hlöðufell, south-west Iceland: a history of ice-confinement. *Journal of Volcanology and Geothermal Research* 185:276–289.

Slater, L., Jull, M., McKenzie, D., Grönvold, K., 1998. Deglaciation effects on mantle melting under Iceland: results from the northern volcanic zone. *Earth and Planetary Sciences Letters* 164:151–154.

Slunga, R., Rögnvaldsson, S.T., Bödvarsson, R., 1995. Absolute and relative locations of similar events with application to microearthquakes in southern Iceland. *Geophysical Journal International* 123, 409–419.

Smellie, J.L., 2008. Basaltic subglacial sheet-like sequences: evidence for two types with different implications for the inferred thickness of associated ice. *Earth Science Reviews* 88:60–88.

Smellie, J.L. (2000) Subglacial eruptions. In: Sigurdsson, H (ed) *Encyclopedia of volcanoes*. Academic, San Diego, pp 403–418.

Smellie, J.L., Mcintosh, W.C., Esser, R., Fretwell, P., 2006. The Cape Purvis volcano, Dundee Island (northern Antarctic Peninsula): late Pleistocene age, eruptive processes and implications for a glacial palaeoenvironment. *Antarctic Sciences* 18, 399–408.

Smellie, J.L., Skilling, I.P., 1994. Products of subglacial volcanic eruptions under different ice thicknesses: two examples from Antarctica. *Sedimentary Geology* 91, 115–129.

Stefánsson, R., Bödvarsson, R., Slunga, R., Einarsson, P., Jakobsdottir, S.S., Bungum, H., Gregersen, S., Havskov, J., Hjelme, J., Korhonen, H., 1993. Earthquake prediction research in the South Iceland Seismic Zone and the SIL project. *Bulletin of the Seismological Society of America* 83, 696–716.

Sternai, P., Caricchi, L., Castelltort, S., Champagnac, J.D., 2016. Deglaciation and glacial erosion: a joint control on the magma productivity by continental unloading. *Geophysical Research Letters* 43, 1632–1641.

Stewart, I.A., Sauber, J.M., Rose, J. 2000 Glacio-seismotectonics: Ice sheets, crustal deformation and seismicity. *Quaternary Science Reviews* 19(14–15):1367–1389. DOI: 10.1016/S0277-3791(00)00094-9

Striberger, J., Björck, S., Holmgren, S., Hamerlik, L., 2012. The sediments of Lake Lögurinn—a unique proxy record of Holocene glacial meltwater variability in eastern Iceland. *Quaternary Science Reviews* 38, 76–88.

Sturkell, E., Einarsson, P., Sigmundsson, F., Hreinsdóttir, S., Geirsson, H., 2003. Deformation of Grímsvötn volcano, Iceland: 1998 eruption and subsequent inflation. *Geophysical Research Letters*, 30, 1182–1185. doi: 10.1029/2002GL016460

Svendsen, J.I., Gataullin, V., Mangerud, J., Polyak, L., 2004. The glacial history of the Barents and Kara Sea region. In: Ehlers, J., Gibbard, P. (Eds.), *Quaternary Glaciations—Extent and Chronology, Vol. 1*. Elsevier, Amsterdam.

Toucanne, S., Zaragosi, S., Bourillet, J.F., Cremer, M., Eynaud, F., Van Vliet-Lanoë, B., Penaud, A., *et al*., 2009. Timing of massive "fleuve Manche" discharges over the last 350 kyr: insights into the European ice-sheet oscillations and the European drainage network from MIS 10 to 2. *Quaternary Science Reviews* 28, 1238–1256.

Tuffen, H., Owen, J., Denton, J.S., 2010. Magma degassing during subglacial eruptions and its use to reconstruct palaeo-ice thicknesses. *Earth Sciences Reviews* 99, 1–18.

Van Loon, A.J., 2009. Soft-sediment deformation structures in siliciastic sediments: an overview. *Geologos* 15, 3–55.

Van Vliet-Lanoë, B., Bourgeois, O., Dauteuil, O., Embry, J.C., Guillou, H., Schneider, J.L., 2005. Deglaciation and volcano-seismic activity in Northern Iceland: Holocene and early Eemian (the Syðra Formation). *Geodynamica Acta* 18, 81–100.

Van Vliet-Lanoë, B., Guðmundsson, Á., Guillou, H., van Loon, A.J., De Vleeschouwer, F., 2010. Glacial Terminations II and I as recorded in NE Iceland. *Geologos* 16, 201–223.

Van Vliet-Lanoë, B., Maygari, A., Meilliez, F., 2004. Distinguishing between tectonic and periglacial deformations of quaternary continental deposits in Europe. *Global and Planetary Change* 43, 103–127.

https://doi.org/10.1017/qua.2019.68 Published online by Cambridge University Press

Van Vliet-Lanoë, B., Schneider, J.L., Guðmundsson, Á., Guillou, H., Nomade, S., Chazot, G., Liorziou, C., Guégan, S., 2018. Eemian estuarine record forced by glacio-isostasy (S Iceland)—link with Greenland and deep sea records. *Canadian Journal of Earth Sciences* 55, 154–171.

Van Vliet-Lanoë, B., Van Cauwenberge, A.-S., Bourgeois, O., Dauteuil, O., Schneider, J.L., 2001. A candidate for the Last Interglacial record in northern Iceland: the Syðra Formation. Stratigraphy and sedimentology. *Compte-Rendu de l'Académie des Sciences Paris* 332, 577–584.

van Kreveld, S., Sarthein, M., Erlenkeuser, H., Grootes, P., Jung, S., Nadeau, M.J., Pflaumann, U., Voelker, A., 2000. Potential links between surging ice sheets, circulation changes, and the Dansgaard-Oeschger cycles in the Irminger Sea, 60–18 ka. *Paleoceanography* 15, 425–442.

Voelker, A., Haflidason, H., 2015. Refining the Icelandic tephra chronology of the last glacial period—the deep-sea core PS2644 record from the southern Greenland Sea. *Global and Planetary Change* 131, 35–62.

Walker, G.P.L., 1965. Acid volcanic rocks in Iceland. *Bulletin of Volcanology* 29, 375–402.

Watt, S.-F.-L., Pyle, D.-M., Mather, T.-A., 2013. The volcanic response to deglaciation: evidence from glaciated arcs and a reassessment of global eruption records. *Earth Science Reviews*122, 77–102.

Werner, R., Schmincke, H.U., Sigvaldason, G.E., 1996. A new model for the evolution of table mountains: volcanological and petrological evidence from Herdubreid and Herdubreidartogl volcanoes (Iceland). *Geologisch Rundschau* 85, 390–397.

Wu, P., Hasegawa, H., 1996. Induced stresses and fault potential in Eastern Canada due to a realistic load: a preliminary analysis. *Geophysical Journal International* 127, 215–229.

Wylie, J.J., Helfrich, K.R., Dade, B., Lister, J.R., Salzig, J.F., 1999. Flow localization in fissure eruptions. *Bulletin of Volcanology* 60, 432–440.

Zielinksi, G., 2000. Use of paleo-records in determining variability within the volcanism–climate system. *Quaternary Science Reviews* 19, 417–438.

Zimbelman, J.R., Gregg, T.K.P., 2000 Environmental effects on volcanic eruptions: From deep oceans to deep space, Kluwer Academic/Plenum, New York.

https://doi.org/10.1017/qua.2019.68 Published online by Cambridge University Press